



HAL
open science

A model of on/off transitions in neurons of the deep cerebellar nuclei: deciphering the underlying ionic mechanisms

Hugues Berry, Stéphane Genet

► **To cite this version:**

Hugues Berry, Stéphane Genet. A model of on/off transitions in neurons of the deep cerebellar nuclei: deciphering the underlying ionic mechanisms. *Journal of Mathematical Neuroscience*, 2021, 11 (1), pp.1-34. 10.1186/s13408-021-00105-3 . hal-03190183

HAL Id: hal-03190183

<https://hal.sorbonne-universite.fr/hal-03190183>

Submitted on 6 Apr 2021

HAL is a multi-disciplinary open access archive for the deposit and dissemination of scientific research documents, whether they are published or not. The documents may come from teaching and research institutions in France or abroad, or from public or private research centers.

L'archive ouverte pluridisciplinaire **HAL**, est destinée au dépôt et à la diffusion de documents scientifiques de niveau recherche, publiés ou non, émanant des établissements d'enseignement et de recherche français ou étrangers, des laboratoires publics ou privés.

RESEARCH

Open Access



A model of on/off transitions in neurons of the deep cerebellar nuclei: deciphering the underlying ionic mechanisms

Hugues Berry^{1,2} and Stéphane Genet^{3*}

*Correspondence:

stephane.genet@upmc.fr

³Sorbonne Université, CNRS, Institut des Systèmes Intelligents et de Robotique, ISIR, F-75005 Paris, France

Full list of author information is available at the end of the article

Abstract

The neurons of the deep cerebellar nuclei (DCNn) represent the main functional link between the cerebellar cortex and the rest of the central nervous system. Therefore, understanding the electrophysiological properties of DCNn is of fundamental importance to understand the overall functioning of the cerebellum. Experimental data suggest that DCNn can reversibly switch between two states: the firing of spikes (F state) and a stable depolarized state (SD state). We introduce a new biophysical model of the DCNn membrane electro-responsiveness to investigate how the interplay between the documented conductances identified in DCNn give rise to these states. In the model, the F state emerges as an isola of limit cycles, i.e. a closed loop of periodic solutions disconnected from the branch of SD fixed points. This bifurcation structure endows the model with the ability to reproduce the F → SD transition triggered by hyperpolarizing current pulses. The model also reproduces the F → SD transition induced by blocking Ca currents and ascribes this transition to the blocking of the high-threshold Ca current. The model suggests that intracellular current injections can trigger fully reversible F ↔ SD transitions. Investigation of low-dimension reduced models suggests that the voltage-dependent Na current is prominent for these dynamical features. Finally, simulations of the model suggest that physiological synaptic inputs may trigger F ↔ SD transitions. These transitions could explain the puzzling observation of positively correlated activities of connected Purkinje cells and DCNn despite the former inhibit the latter.

Keywords: Deep cerebellar nuclei; State transition; Biophysical model

1 Introduction

The connectivity of the cerebellum places deep cerebellar nuclei neurons (DCNn) in a strategic position. Their axons are the main output of the cerebellum, projecting to the forebrain, the brain stem and the spinal cord. In turn, DCNn are the main target of the Purkinje cell (PC) axons, which are themselves the sole output system of the cerebellar cortex. As noted by Llinás and Muhlethaler [1] the cerebella nuclear cells are therefore the main functional link between the cerebellar cortex and the rest of the central nervous system. It follows that a detailed understanding of electrophysiological properties of the DCNn is one of the fundamental prerequisites to understanding the overall functioning

© The Author(s) 2021. This article is licensed under a Creative Commons Attribution 4.0 International License, which permits use, sharing, adaptation, distribution and reproduction in any medium or format, as long as you give appropriate credit to the original author(s) and the source, provide a link to the Creative Commons licence, and indicate if changes were made. The images or other third party material in this article are included in the article's Creative Commons licence, unless indicated otherwise in a credit line to the material. If material is not included in the article's Creative Commons licence and your intended use is not permitted by statutory regulation or exceeds the permitted use, you will need to obtain permission directly from the copyright holder. To view a copy of this licence, visit <http://creativecommons.org/licenses/by/4.0/>.

of the cerebellum. Several experimental studies have demonstrated that DCNn are not simple leaky integrators of their synaptic inputs but exhibit a repertoire of intrinsic active electric properties. Recordings using sharp electrodes or patch clamps have evidenced that isolated DCNn are spontaneously active, producing pacemaker firing of fast spikes at a low frequency of about 20 Hz [2–7]. DCNn also exhibit rebound depolarizing potentials at break of a hyperpolarizing current pulse in a variety of preparations (see [3]). In addition, Jahnsen [2] reported that pulses of injected hyperpolarizing current can switch DCNn from their spontaneous firing state to a silent mode of activity. As this silent mode was observed to persist over time spans >1 s, Jahnsen's results putatively point at the existence of a stable point attractor in the DCNn phase space. Moreover, the observation of Jahnsen that a subsequent hyperpolarizing pulse can switch the DCNn back to their spontaneous firing activity (see Fig. 5 in [2]) suggests that transitions between the two modes of activity are reversible. Reversible transitions between spontaneous firing and a silent depolarized state were also reported later by Raman *et al.* [4] in patch-clamp recordings of DCNn, thus ruling out the possibility that these transitions are artifacts resulting from experimental membrane leaks created by sharp electrodes used by Jahnsen. While sparse, these experimental results hint at the coexistence of two different stable electric states in the DCNn phase space: a silent depolarized state (stable fixed point, sFP) and an active state characterized by low frequency firing of large-amplitude spikes (stable limit cycle, sLC).

Such dynamics was early predicted as possible solutions of the Hodgkin–Huxley (HH) model of the action potential by Cooley *et al.* as early as 1965 [8]. They pointed out that (i) if the HH model had only two variables, the surrounding of the sFP by the orbit of the sLC (see Theorem 6.2 in Grimshaw [9]) would imply the existence of an unstable limit cycle (uLC) to separate the basins of attraction of the two ω -limit sets but (ii) that the existence of such an uLC is not a necessary condition for the (four-dimensional) HH model to exhibit such dynamics. Hassard and Shiau [10] and Rinzel and Miller [11] subsequently showed that the HH model has actually a branch of unstable limit cycles in addition to the branch of limit cycles in the range of input currents where the sFP and the sFP coexist. Moreover Guttman *et al.* [12] subsequently proved the physiological soundness of the premises of Cooley *et al.* [8] by reporting that the squid axon can be switched by short pulses of electric current between a silent mode and a firing mode. They also went beyond Cooley *et al.* [8] by suggesting that, since the HH model has a four-dimensional phase space, the basins of attraction of the sFP and the sLC are separated by a $d \geq 2$ manifold rather than by a single curve and that this separatrix presumably contains the previously identified uLC.

These conjectures deserve explanation. Firstly, uniqueness of the solution of a Cauchy problem for systems of ordinary differential equations (ODE) imply that, in a 2D phase space, the separatrix between a sLC and a sFP must be a Jordan curve, say C , obviously corresponding to a limit cycle solution of the system. Secondly, this limit cycle must be unstable to ensure that all solutions starting from the interior (*resp.* exterior) of C converge onto the sFP (*resp.* the sLC). A limit cycle always has one of its Floquet exponents $\rho_1 = 1$ (see e.g. [13], p. 223) and, for a 2D system, its second exponent ρ_2 is >1 if the limit cycle is unstable. The local stable and unstable manifolds of the uLC are, respectively, spanned by ρ_1 and ρ_2 and both have dimension 1. According to the stable manifold theorem for periodic orbits (see [13], p. 220), the global stable (*resp.* unstable) manifolds of the uLC have the same respective dimensions as the local stable (*resp.* unstable) manifolds of the uLC.

It is therefore tempting to conjecture that, in systems with dimension >2 , the separatrix is also the global stable manifold of the uLC, that is a manifold with dimension $k + 1$ with k being the number of Floquet exponents <1 . Such a manifold may have a complicated shape. But if solutions are bounded, the simplest manifold achieving separation of the attraction basins of the sFP and sLC would be a closed manifold (i.e. compact and without bounds). Characterizing the separatrix may have remained a theoretical issue since the coexistence of the sFP and the sLC has, to our knowledge, only been reported in squid axons bathed in non-physiological low Ca salines. However, the observation of such a coexistence in DCNn put this mathematical question into a neurophysiological context since characteristics of the separatrix obviously constrain the types of stimuli capable to trigger sFP \leftrightarrow sLC state changes.

The repertoire of membrane conductances expressed by DCNn has been the subject of several studies. These conductances comprise two calcium carried currents [14], a non-inactivating high-threshold Ca current (I_{CaH}) and an inactivating (transient) one (I_{CaT}) and a calcium-dependent potassium current (I_{KCa} , [15]). In addition, Raman *et al.* [4] have identified a tonic non-cationic current, I_{TCN} . However, in spite of these characterizations, we still lack an understanding of how this set of conductances actually implements the intrinsic properties of the DCNn. In the absence of a theoretical framework, it is difficult to relate the response of the DCNn membrane voltage to its active conductances. In particular, several of the available experimental observations raise unsolved issues. For instance, transitions from the spontaneous firing state to the silent depolarized one can be triggered by inhibition of the calcium currents I_{CaH} and I_{CaT} [4] but it is not clear whether the inhibition must concern both currents or only one of them. Likewise, it is not known if the transitions observed *in vitro* using current pulse injection are also triggered by synaptic currents.

Biophysical models have proven highly useful to understand how active conductances interact to underpin active electrical signals in neurons. For instance, the acclaimed Hodgkin and Huxley model of the action potential in the squid axon has proved a very powerful approach to our understanding of the generation of action potentials [16]. For DCNn, the only detailed (compartmental) biophysical model of DCNn thus far (to our knowledge) has been proposed in a pioneer study by Steuber *et al.* [7]. The more recent model of Sudhakar *et al.* [17] actually adopts the structure and equations of the Steuber *et al.*'s model and only uses different values for the densities of active conductances. However, neither of these articles evidences capabilities of this model to reproduce state transitions experimentally observed by Jahnsen [2] and Raman *et al.* [4]. Moreover, the Steuber *et al.*'s model relies on several assumptions which experimental support can be questioned. Thus, it assumes that DCNn express two different Hodgkin–Huxley-type voltage-dependent Na currents, a fast one and a slowly inactivating one (i.e. persistent). Expression of a persistent Na current by DCNn was postulated by Jahnsen [2] and Llinás and Muhlethaler [1] and its existence has since been confirmed by two experimental studies (Raman *et al.* [4] and Afshari *et al.* [18]). However, these studies suggest that the persistent Na current belongs to the class of so-called resurgent Na currents (Raman and Bean, [19]). Resurgent currents involve a specific mode of channel aperture whose faithful modeling requires a set of 12 ODEs (Raman and Bean, [19]). Moreover, the Steuber *et al.*'s model assumes a non-uniform distribution of active conductances between the dendrites and soma of DCNn which remained to be proved (with the exception of T Ca channels that cluster to

the soma and proximal dendrites of DCNn; see McKay et al. [20]). Here we propose a new biophysical model of DCNn electrogenesis. To allow mathematical analysis of the model, we focus on an isopotential (non-compartmental) description, in which the DCNn membrane potential evolves under the influence of the 6 conductances mentioned above (I_{NaV} , I_{Kdr} , I_{CaH} , I_{CaT} , I_{KCa} , and I_{TCN}). Spontaneous firing of fast spikes emerges in the model as an isola of limit cycles in a range of driving currents. Within this range, the model exhibits another coexisting stable attractor: a stable depolarized stationary-state. Owing to this peculiar bifurcation structure, the model reproduces the transitions between spontaneous firing and a silent state that have been reported experimentally [2, 4]. Like in these experimental reports, the transitions in the model can be triggered by hyperpolarizing current pulses or by blocking Ca currents in the absence of hyperpolarization. Analysis of the model suggests that the latter transition is specifically due to the inhibition of the I_{CaH} current. Finally, simulations of the model suggest that physiological synaptic inputs may trigger the state transitions.

2 Methods

It is currently unknown whether DCNn are electrically compact neurons nor whether their ion channels have non-uniform distributions over their membrane surface (with the exception of high threshold voltage-dependent Ca channels [14]). In the absence of evidence for a functional role of these heterogeneities, we chose to build an isopotential model of DCNn to (i) investigate the hypothesis that DCNn have two coexisting stable states of activity, (ii) identify the interactions between the active membrane ion currents that are responsible for this electric feature and (iii) investigate whether physiological inputs could trigger transitions between these states. DCNn do not form a homogeneous population from the phenotypic standpoint. Their population has been divided into two classes (see [21] for an introduction) which partially correlate with the location of their target neurons. Glutamatergic DCNn project excitatory inputs to motor centers in the brain stem, the mesencephalon, the thalamus and pre-cerebellar nuclei through the mossy fiber pathway. GABAergic DCNn achieve inhibitory synapses on neurons of the inferior olive [22] and glutamatergic DCNn [23]. A class of rare small-sized DCNn has also been identified [24]. In addition to their neurotransmitters and projection sites, these classes of neurons can also express different sets of ion channels [25]. However, it is unknown to what extent their intrinsic electrophysiological properties are heterogeneous. In the absence of this information, we propose below a generic model for the electrogenesis of DCNn.

2.1 State variables and equations of the model

Our standard model has 6 state variables. The dynamics of these variables is governed by 6 associated ordinary differential equations (ODE) that we describe below. The two main state variables of the model are the membrane potential, V (mV), and the cytoplasmic concentration of free Ca^{2+} ions $[Ca]$ (μM). Their respective ODE read

$$C \frac{dV}{dt} = - \sum_i I_i^{\text{ion}} + I_S \quad (1)$$

and

$$\frac{d[Ca]}{dt} = -\frac{10^2(I_{CaH} + I_{CaT})R_c/F + 2k([Ca] - [Ca]_b)(R_c - \delta)}{\delta(2R_c - \delta)\left[1 + \frac{B_T}{K_D(1 + \frac{10^{-11}[Ca]}{K_D})^2}\right]} \tag{2}$$

Equation (1) is standard for biophysical models of neurons (see e.g. [26]). It can be derived from the first Kirchhoff law of electromagnetism which states that electric charges can neither be created nor destroyed. The set of membrane ion currents I_i^{ion} (nAcm⁻²) appearing in Eq. (1) is detailed below. For the input current I_S we distinguish tonic (I_{DC}) and phasic (I_φ) components and write $I_S = I_{DC} + I_\varphi$. The phasic component was written as the product of an ohmic term $g_\varphi(V - E_\varphi)$ and the product of two Heaviside step functions of time $H(t - t_{start})H(t_{end} - t) = \begin{cases} 1 & \text{for } start < t < end, \\ 0 & \text{elsewhere.} \end{cases}$ The ODE for the cytoplasmic free calcium ions concentration (Eq. (2)) is a balance equation. The source term corresponds to calcium ions entry into the cytoplasm through membrane channels underlying the I_{CaH} and I_{CaT} currents. The sink term corresponds to the extrusion of cytoplasmic Ca²⁺ ions by cytoplasmic membrane pumps and their internalization by Ca pumps in the endoplasmic reticulum membrane, both processes being modeled with a simple linear term. The ODE actually includes a second sink term corresponding to Ca²⁺ ions buffering by Ca-binding proteins. It appears as the denominator of the right-hand side of Eq. (2) owing to the hypothesis that the binding of Ca²⁺ ions is very fast (see [27] for the derivation of Eq. (2) and Table 1 for parameter values).

The ion membrane conductances (for currents obeying the Nernst equation) and permeabilities (for currents obeying the Goldman constant-field equation) were modeled as the product of a maximum conductance \bar{g} ($\mu S/cm^2$) or permeability \bar{P} (cm/s) and either the product of voltage-dependent activation and inactivation variables m and h or a Ca-dependent variable w , i.e.

$$\begin{aligned} g(P) &= \bar{g}(\bar{P})m^p h^q, \\ g(\bar{P}) &= \bar{g}(\bar{P})w, \end{aligned} \tag{3}$$

in which p and q are integers. The remaining four states variables of the model correspond to in(activation) variables of ion currents I_{NaV} , I_{Kdr} and I_{CaT} and namely are h_{NaV} , m_{Kdr} , m_{CaT} and h_{CaT} . Their dynamics obey first order differential equations of the form [16]

$$\forall x \in \{h_{NaV}, m_{Kdr}, m_{CaT}, h_{CaT}\} \frac{dx}{dt} = \frac{x_\infty - x}{\tau_x}, \tag{4}$$

in which x_∞ and τ_x stand for the steady-state value and the exponential time constant of variable x , respectively. The available experimental data on the voltage-dependence in DCNn [4, 18] were insufficient to constrain a fully detailed Hodgkin–Huxley-type model of these currents since they do not document the voltage dependence of rate functions governing state transitions of ion channels. We therefore adopted the modeling approach of Huguenard and McCormick [29] in which x_∞ and τ_x are considered as independent functions of V (however, see the discussion) of the form

$$x_\infty = \frac{1}{1 + e^{\pm(V-V_x)/k_x}}, \tag{5}$$

Table 1 List of parameter values. The abbreviation ‘cstd’ indicates that the value was constrained to reproduce experimental dynamics of DCN

| Parameter | Value | Reference |
|--|---|---|
| <i>Calcium ions dynamics</i> | | |
| R_c | 5×10^{-4} cm | [26] |
| δ | 3×10^{-4} cm | |
| k | 10^{-2} cm/s | |
| $[B]_T$ | 1.5×10^2 μ M | |
| K_D | 1 μ M | |
| <i>Membrane potential dynamics</i> | | |
| C | 1 μ F/cm ² | [25] |
| <i>Membrane ion currents</i> | | |
| <i>Maximum conductances and permeabilities</i> | | |
| g_L | 2×10^1 μ S/cm ² | cstd |
| g_{NaV} | 5×10^3 μ S/cm ² | |
| g_{Kdr} | 4.5×10^3 μ S/cm ² | |
| g_{TCN} | 4.5×10^1 μ S/cm ² | |
| g_{KCa} | 10 μ S/cm ² | |
| P_{CaH} | 2×10^{-4} cm/s | |
| P_{CaT} | 7×10^{-4} cm/s | |
| <i>Nernst potential</i> | | |
| E_L | -60 mV | cstd |
| E_{Na} | +86 mV | [4] |
| E_K | -80 mV | -83 mV in [28] |
| E_{Cl} | -75 mV | -75 mV [2] and -74.3 mV in [28]; however, see [5] |
| E_{TCN} | -34 mV | [4] |
| <i>Steady-state (in)activation parameters (mV)</i> | | |
| V_{mNaV} | -32 | cstd |
| k_{mNaV} | 8.5 | |
| V_{hNaV} | -55 | |
| k_{hNaV} | 5.5 | [4] |
| V_{mKdr} | -25 | [29] |
| k_{mKdr} | 11.5 | |
| V_{mCaH} | -22 | cstd |
| k_{mCaH} | 4.53 | |
| V_{mCaT} | -56 | [30] |
| k_{mCaT} | 6.2 | |
| V_{hCaT} | -80 | |
| k_{hCaT} | 4 | |
| <i>Parameters of time constants</i> | | |
| τ_{nKdr0} | 0 s | cstd |
| τ_{nKdr1} | 5.4×10^{-3} s | |
| $\alpha\tau_{nKdr}$ | 6×10^{-1} | |
| $V_{\tau_{nKdr1}} = V_{\tau_{nKdr2}}$ | -30 mV | |
| $k_{\tau_{nKdr1}} = k_{\tau_{nKdr2}}$ | 25 mV | |
| τ_{hNaV0} | 5×10^{-3} s | |
| τ_{hNaV1} | 3×10^{-2} s | |
| $\alpha\tau_{hNaV}$ | 1 | |
| $V_{\tau_{hNaV1}} = V_{\tau_{hNaV2}}$ | -65 mV | |
| $k_{\tau_{hNaV1}} = k_{\tau_{hNaV2}}$ | 7 mV | |
| τ_{mCaT0} | 2×10^{-4} s | [30] |
| τ_{mCaT1} | 3.33×10^{-4} | |
| $V_{\tau_{mCaT1}}$ | -131 mV | |
| $k_{\tau_{mCaT1}}$ | 16.7 mV | |
| $\alpha\tau_{mCaT}$ | 1 | |
| $V_{\tau_{mCaT2}}$ | -15.8 mV | |
| $k_{\tau_{mCaT2}}$ | 18.2 mV | |

Table 1 (Continued)

| Parameter | Value | Reference |
|---|------------------------|---|
| τ_{hCaH^0} | 1.2×10^{-2} s | cstd (to produce a C^1 function for τ_{hCaT}) |
| τ_{hCaH^1} | 2 s | |
| $\alpha_{\tau_{hCaT}}$ | 1 | |
| $V_{\tau_{hCaH^1}} = V_{\tau_{hCaH^2}}$ | -81 mV | |
| $k_{\tau_{hCaH^1}} = k_{\tau_{hCaH^2}}$ | 8 mV | |

$$\tau_x = \tau_{x0} + \frac{\tau_{x1}}{e^{\pm(V-V_{\tau_{x1}})/k_{\tau_{x1}}} + \frac{\alpha_{\tau_x}}{e^{(V-V_{\tau_{x2}})/k_{\tau_{x2}}}}} \tag{6}$$

Equation (5) is a so-called Boltzmann function in which the ‘-’ and ‘+’ signs hold, respectively, for the inactivation (h_{NaV} , h_{CaT}) and the activation (m_{Kdr} , m_{CaT}) variables. V_x and k_x are referred to as half-activation potentials and activation slopes of the variable x , respectively. Equation (6) is standard for reproducing the bell-shape of the activation time constant of voltage-dependent currents [29]. The parameter τ_{x0} accounts for the observation that $\lim_{V \rightarrow +\infty} \tau_x > 0$ for the inactivation variable of some particular currents (e.g. I_{Na} in the squid giant axon [11]). The α_{τ_x} parameter allows one to introduce asymmetry in the shape of the time constant as observed for some currents (see e.g. [26], p. 48). We give below a detailed account of the model equation for each of the currents.

I_{NaV} : As in most neurons studied so far, the spikes of the DCNn are blocked by tetrodotoxin (TTX) [4] suggesting that the depolarizing phase of these spikes is underlain by a Hodgkin–Huxley-type of voltage-dependent Na current, I_{NaV} . For this reason, we used the classical Hodgkin–Huxley formalism to model I_{NaV} in DCNn. However, the time constant of m_{NaV} in neurons is usually much smaller than that of h_{NaV} . We therefore used the classical quasi-steady-state approximation replacing m_{NaV} by its steady-state value $m_{NaV\infty}$ (see e.g. [31]). Llinás and Muhlethaler [1] initially suggested that I_{NaV} in DCNn could have a persistent component. Afshari *et al.* [18] have confirmed that I_{NaV} in DCNn has a persistent component that they attribute to the mechanism of resurgent current initially identified in cerebellar Purkinje cells [19]. Given that the resurgent component only amounts to <4% of the total I_{NaV} in DCNn [18] and that a faithful modeling of I_{NaV} endowed with resurgence properties requires a set of 12 ODE [19], we chose to not introduce (see, however, the Discussion) a persistent I_{NaV} in our model and we rather used a classical Hodgkin–Huxley I_{NaV}

$$I_{NaV} = \bar{g}_{NaV} m_{NaV\infty}^3 h_{NaV} (V - E_{Na}), \tag{7}$$

where $m_{NaV\infty}$ is given by Eq. (5) and h_{NaV} by Eqs. (4)–(6).

I_{Kdr} : voltage-dependent K currents of the Kv3-type exhibit fast activation allowing ~1 ms-duration Na spikes in several neuron types [32]. Llinás and Muhlethaler [1] report spike duration (measured at half-width) ranging from 0.44 to 0.7 ms in DCNn suggesting that spike repolarization in these neurons is achieved by Kv3 channels. Raman *et al.* [4] have dissected out a high-threshold voltage-dependent potassium current in DCNn that is presumably involved in the repolarization of their spikes. The activation time constant of this current (12 ms at +12 mV) is too large for Kv3 channels and rather points to the Kv2 family of K channels [33]. However, Raman *et al.* [4] only used 1 mM TEA whereas to

block voltage-dependent K channels whereas blocking Kv2 channels require several millimolar concentration of TEA to block [34]. Moreover, no molecular study has yet, to our knowledge, demonstrated expression of Kv2 channels in DCNn. On the opposite, several studies have shown that DCNn express all four Kv3 subunits (see e.g. [35] and [32]) and the electrophysiological study of Lamont [28] suggests that Kv3 channels in DCNn are functional. DCNn can fire spikes at frequencies up to >100 Hz which seem unattainable with Kv2 serving to repolarize spikes. Owing to these findings, our model assumes that I_{Kdr} is carried by fast-activating K channels (however, see the discussion for the involvement of putative Kv2 channels),

$$I_{Kdr} = \bar{g}_{Kdr} m_{Kdr}^4 (V - E_K), \tag{8}$$

where m_{Kdr} is given by Eqs. (4)–(6). The parameters from this current were taken from a model of Purkinje cell dendrite [27].

I_{TCN} : There is experimental evidence for a TTX-insensitive current in DCNn that can depolarize them beyond their spike threshold [4], this current being tonic (i.e. V -independent) and non-selective for cations [4]. We modeled this current using Ohm’s law with a constant conductance, i.e. as an effective leak current:

$$I_{TCN} = g_{TCN}(V - E_{TCN}). \tag{9}$$

Calcium currents I_{CaH} and I_{CaT} : Owing to the large gradient of Ca^{2+} ions across the cytoplasmic membrane of neurons (typically $[Ca]_o/[Ca]_i \simeq 2 \times 10^5$ in a neuron at rest), voltage-dependent Ca currents are not adequately modeled by the Nernst equation. This equation accurately describes ion fluxes only close to thermodynamic equilibrium (see e.g. [26]). Far from equilibrium, Ca currents exhibit a rectification in their I/V relation which is well accounted for by the constant-field equation of Goldman (see e.g. Chap. 13 in [26]). We therefore used this equation to describe Ca currents in our model. As mentioned above, two types of Ca currents have been identified in DCNn [14]: a non-inactivating high-threshold current I_{CaH} and an inactivating current I_{CaT} . Both currents are given by

$$I_{Ca_x} = \frac{P_{Ca_x}(zF)^2 V}{RT(1 - \alpha(V))} ([Ca] - \alpha(V)[Ca]_o), \tag{10}$$

where $Ca_x \in \{CaT, CaH\}$ and $\alpha(V) = e^{-\frac{2FV}{RT}}$. A temperature $T = 298$ K was used in all simulations. The molecular identity of ion channels underlying I_{CaH} in DCNn is currently not precisely known. Gauck *et al.* [14] have shown that a large fraction of I_{CaH} in DCNn is non-inactivating and is therefore likely composed of L-, T- or R-type currents. They have also observed that a small fraction of I_{CaH} inactivates, thereby also indicating the presence of N-type calcium channels. For the sake of simplicity and since L-type calcium channels open as quickly as N-types channels in neurons [36], we derived a simple equation for P_{CaH} by assuming that it activates instantaneously and does not inactivate, i.e.

$$P_{CaH} = \bar{P}_{CaH} m_{CaH\infty}, \tag{11}$$

where $m_{CaH\infty}$ is given by Eq. (5).

Setting an equation for I_{CaT} proved more challenging. Indeed, this current can be underlain by three isoforms of calcium channels, Cav3.1, Cav3.1 and Cav3.3 which have marked different time constants for both activation and inactivation [18]. Molineux *et al.* [25] have demonstrated the expression of Cav3.1 in both GABAergic and non-GABAergic DCNn, whereas Cav3.3 expression is restricted to non-GABAergic DCNn. Since both types of DCNn exhibit rebound properties, these findings suggest that the expression of Cav3.1 is sufficient to generate a rebound in both cell types. McKay *et al.* [20] have shown that Cav3.1 channels are largely confined to the soma of the DCNn. McRory *et al.* [30] have found that both τ_{act} and τ_{inact} of Cav3.1–3 channels decay monotonically with voltage toward a voltage-independent nonzero minimum. This feature is well reproduced by the thalamic I_{CaT} model of Destexhe *et al.* [37] which we adopted here for the DCNn. Its permeability equation reads

$$P_{CaT} = \bar{P}_{CaT} m_{CaT}^2 h_{CaT}, \tag{12}$$

where m_{CaT} and h_{CaT} are given by Eqs. (4)–(6). Nevertheless, we had to adapt the original model of Destexhe *et al.* [37] to provide a faithful account of I_{CaT} in DCNn. Firstly, we adapted the values of the time constants $\tau_{m_{CaT}}$ and $\tau_{h_{CaT}}$ of the original model to match the properties of the Cav3.1 channels expressed by DCNn [25]. Secondly, the model by Destexhe *et al.* uses a discontinuous piecewise function to describe $\tau_{h_{CaT}}$. This prevents guaranteeing existence and uniqueness of the solutions of the model according to the Cauchy-Lipschitz theorem (see e.g. [38]). We therefore replaced the original formulation of $\tau_{h_{CaT}}$ in Destexhe *et al.* by the continuous and differentiable formulation of Eq. (6).

I_{KCa} : The DCNn express calcium-dependent potassium currents of the SK (small-conductance) type [25]. Those potassium-specific channels are gated by calcium according to a Hill-type equation (see e.g. [39])

$$I_{KCa} = g_{KCa} w_{KCa} (V - E_K) \tag{13}$$

which assumes instantaneous gating of SK channels by calcium:

$$w_{KCa} = \frac{[Ca]^5}{C_{KCa}^5 + [Ca]^5}. \tag{14}$$

Finally, the model includes a leakage current. The value of its conductance g_{Leak} was set to a value allowing the model to reproduce the passive time constant of DCNn recorded *in vitro* (as probed by small hyperpolarizing pulses)

$$I_{Leak} = g_{Leak} (V - E_{Leak}). \tag{15}$$

Table 1 lists the standard value of all parameters appearing in Eqs. (5)–(15).

2.2 Boundedness of solutions

We follow the approach of Cronin [40] to prove that all physiologically significant solutions of the model are bounded. Let us first consider the dynamics of state variables h_{NaV} , m_{Kdr} , m_{CaT} and h_{CaT} which all obey ODE of the form of Eq. (4). The function $\tau_{x \in \{h_{NaV}, m_{Kdr}, m_{CaT}, h_{CaT}\}}(V)$ in Eq. (4) is positive whatever the value of V according to Eq. (6).

Moreover, for all physiologically significant initial conditions on V we have $0 < x < 1$ according to Eq. (5). It follows that $\frac{dx}{dt} > 0$ if $x = 0$ and $\frac{dx}{dt} < 0$ if $x = 1$. This implies that all physiological solutions remain in the

$$\left\{ (h_{NaV}, m_{Kdr}, m_{CaT}, m_{CaT}) \left| \begin{array}{l} h_{NaV} \\ m_{Kdr} \\ m_{CaT} \\ m_{CaT} \end{array} \in [0, 1] \right. \right\}$$

region of the model phase space.

Let us now turn to Eq. (1) in the particular case where $P_{CaH} = P_{CaT} = 0$ (namely the model deprived of its Ca currents) and let $E_{max} = \max\{E_{Na}, E_K, E_{Leak}\}$ and $E_{min} = \min\{E_{Na}, E_K, E_{Leak}\}$. Recall then that currents I_{Na} , E_K and E_{Leak} all have the form $I_i = f_i(V)(V - E_i)$, $i \in \{Na, K, Leak\}$ with $0 < f_i(V) < 1$. Then Eq. (1) with $I_S = 0$ implies that $\frac{dV}{dt} > 0$ if $V < E_{min}$ and that $\frac{dV}{dt} < 0$ if $V > E_{max}$. It follows that all physiological solutions remain in the

$$\left\{ (V, h_{NaV}, m_{Kdr}, m_{CaT}, h_{CaT}) \left| V \in [E_{min}, E_{max}], \begin{array}{l} h_{NaV} \\ m_{Kdr} \\ m_{CaT} \\ h_{CaT} \end{array} \in [0, 1] \right. \right\}$$

subset of the phase space.

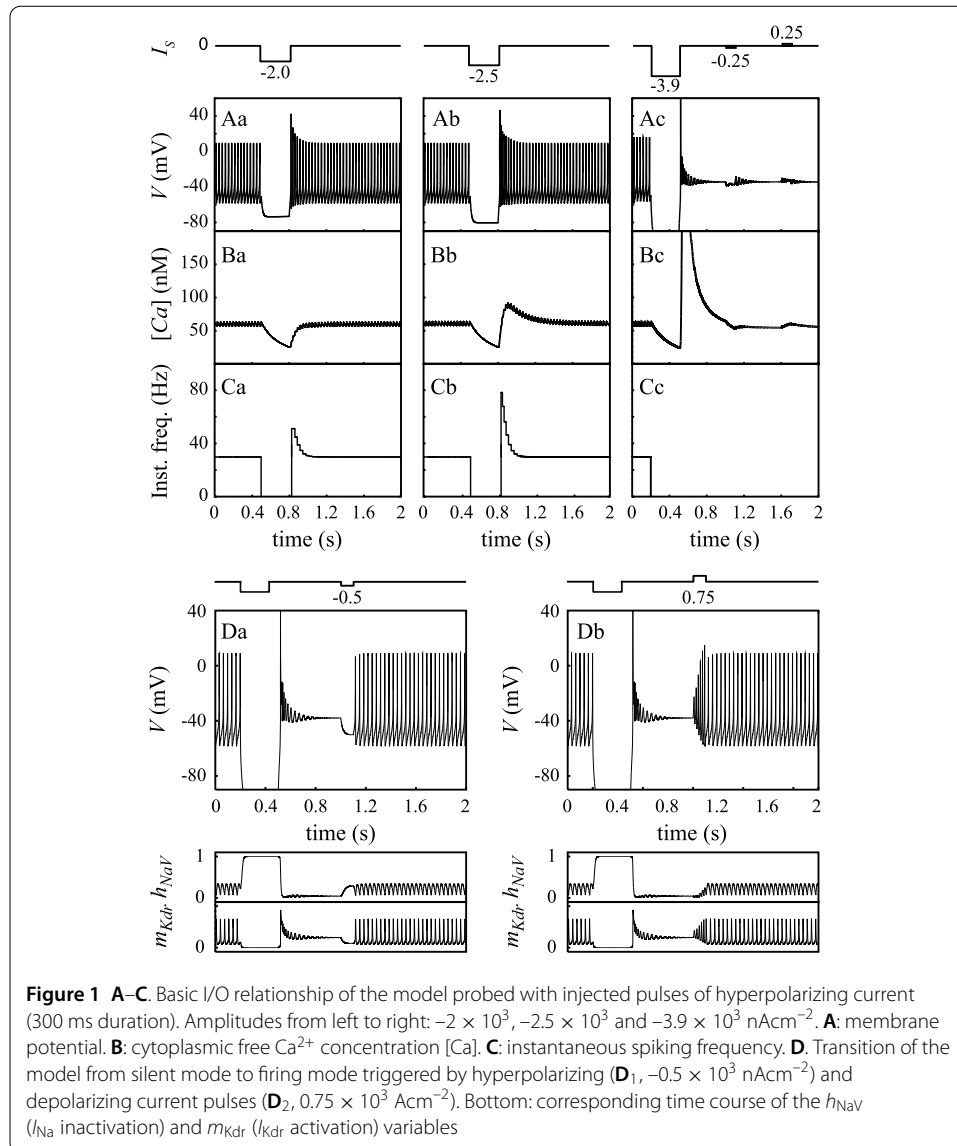
Proof of the boundedness of solutions is finalized by extending the above result to the full model (i.e. including Ca currents) as follows. Let now $E_{max} = \max\{E_{Na}, E_K, E_{Leak}, E_{Ca}\}$ and $E_{min} = \min\{E_{Na}, E_K, E_{Leak}, E_{Ca}\}$. The factor $\alpha(V)$ in Eq. (10) of the Ca currents is easily shown to be positive whatever the value of V . The sign of the $[Ca] - \alpha(V)[Ca]_o$ factor depends on both V and $[Ca]$. Nevertheless, it is easily shown that $I_{Ca} < 0$ for $\{(V, [Ca]) | V < E_{Ca}^{max}, [Ca]_b < [Ca] < [Ca]_o\}$ and positive for $\{(V, [Ca]) | V > E_{Ca}^{max}, [Ca]_b < [Ca] < [Ca]_o\}$ where $E_{Ca}^{max} = \frac{RT}{2F} \ln \frac{[Ca]_o}{[Ca]_b}$. According to Eq. (2), it follows from this last result that $\frac{d[Ca]}{dt} > 0$ if $[Ca] < [Ca]_b$ and $\frac{d[Ca]}{dt} < 0$ if $[Ca] > [Ca]_o$ and therefore that physiologically solutions of the model stay in the set

$$\left\{ (V, Ca, h_{NaV}, m_{Kdr}, m_{CaT}, h_{CaT}) \left| V \in [E_{min}, E_{max}], \begin{array}{l} h_{NaV} \\ m_{Kdr} \\ m_{CaT} \\ h_{CaT} \end{array} \in [0, 1] \right. \right\}$$

3 Results

3.1 Theoretical evidence for two stable states of electric activity in DCNn

Consistent experimental data show that DCNn are pacemaker neurons *in vitro* [2–7]. In the absence of a depolarizing bias current ($I_{DC} = 0$), our neuron model successfully repro-



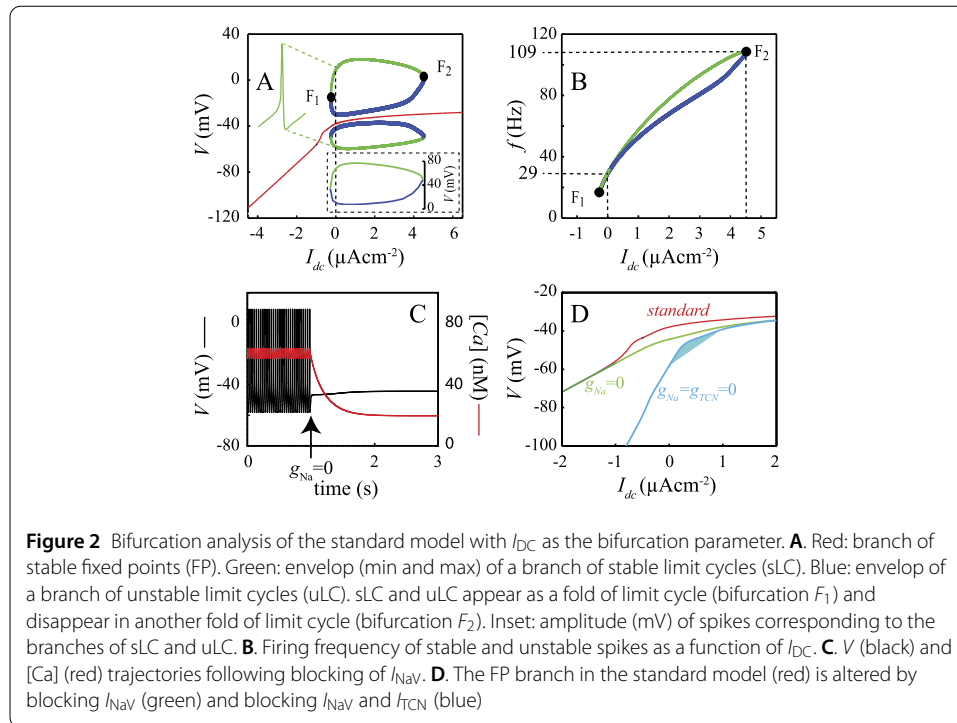
duces this property, with the spontaneous emission of self-sustained fast (~ 1 ms duration) spikes (Fig. 1A₁). We refer to this mode of activity as the firing (F) mode. The spontaneous firing frequency in the model is 28.9 Hz (versus 26 Hz in [2] and ~ 20 Hz in [4]). The amplitude of spontaneous spikes is 67 mV (in the range of extreme values reported experimentally: 57 ± 5 mV in [1] and 82 mV in [4]). As shown in Fig. 1A₁, a 300 ms hyperpolarizing pulse of $-2 \mu\text{Acm}^{-2}$ amplitude interrupts spike firing in the model. Firing resumes at the end of the pulse with an initial phase of increased firing frequency of ~ 200 ms duration (Fig. 1A₁ and C₁). The concentration of free cytosolic calcium [Ca] first decreases during the pulse and quickly recovers its baseline level after the end of the pulse (Fig. 1B₁). Increasing the pulse amplitude shows non-monotonous effects. A moderate increase of the amplitude of the pulse (to e.g. $-2.5 \mu\text{Acm}^{-2}$, Fig. 1A₂–C₂) yields the same behavior, but with a larger transient firing frequency increase at pulse break. The peak frequency during this rebound is close to twice the basal frequency (Fig. 1C₂), in close agreement with the experimental data of Raman *et al.* [4]. We also note the appearance of a rebound

[Ca] increase at the pulse break, which is consistent with the observations of Raman et al. [4] (Fig. 1B₂). Large pulse amplitudes, however, produce a dramatic change of response (Fig. 1A₃–C₃). For instance, a $-3.9 \mu\text{Acm}^{-2}$ pulse triggers a switch of the model to a silent depolarized (SD) state in which the membrane potential settles at -38 mV (Fig. 1A₃). This model feature reproduces the observation of Jahnsen ([2]; see Fig. 5C) that a hyperpolarizing current pulse can switch spontaneously firing DCNn to a silent mode of activity. In the model, the SD state is stable as evidenced by the fact that, once settled in this state, the model remains in this state despite small depolarizing or hyperpolarizing pulses of current (Fig. 1A₃). However, this stability is only local since larger-amplitude hyperpolarizing current pulses (Fig. 1D₁) readily switch the model back to its firing mode. This new behavior is also consistent with the following experimental result by Jahnsen ([2]; see Fig. 5E): when DCNn are switched to the SD state, a subsequent hyperpolarizing pulse can switch them back to the F mode. However, our model extends this finding by showing that depolarizing current should also be able to trigger this transition (Fig. 1D₂). Therefore, our model reproduces the experimental observations that hyperpolarizing pulses can switch the DCNn from their spontaneous low frequency firing (F) state to a stable depolarized (SD) state. The SD state is only locally stable and injection of large hyperpolarizing or depolarizing current pulses switches the DCNn model back to its F state. In the following we provide a mathematical analysis of the model in order to dissect the contribution of the different membrane ion currents to these dynamical features.

3.2 Bifurcation analysis of the model and the silent depolarized state (SD)

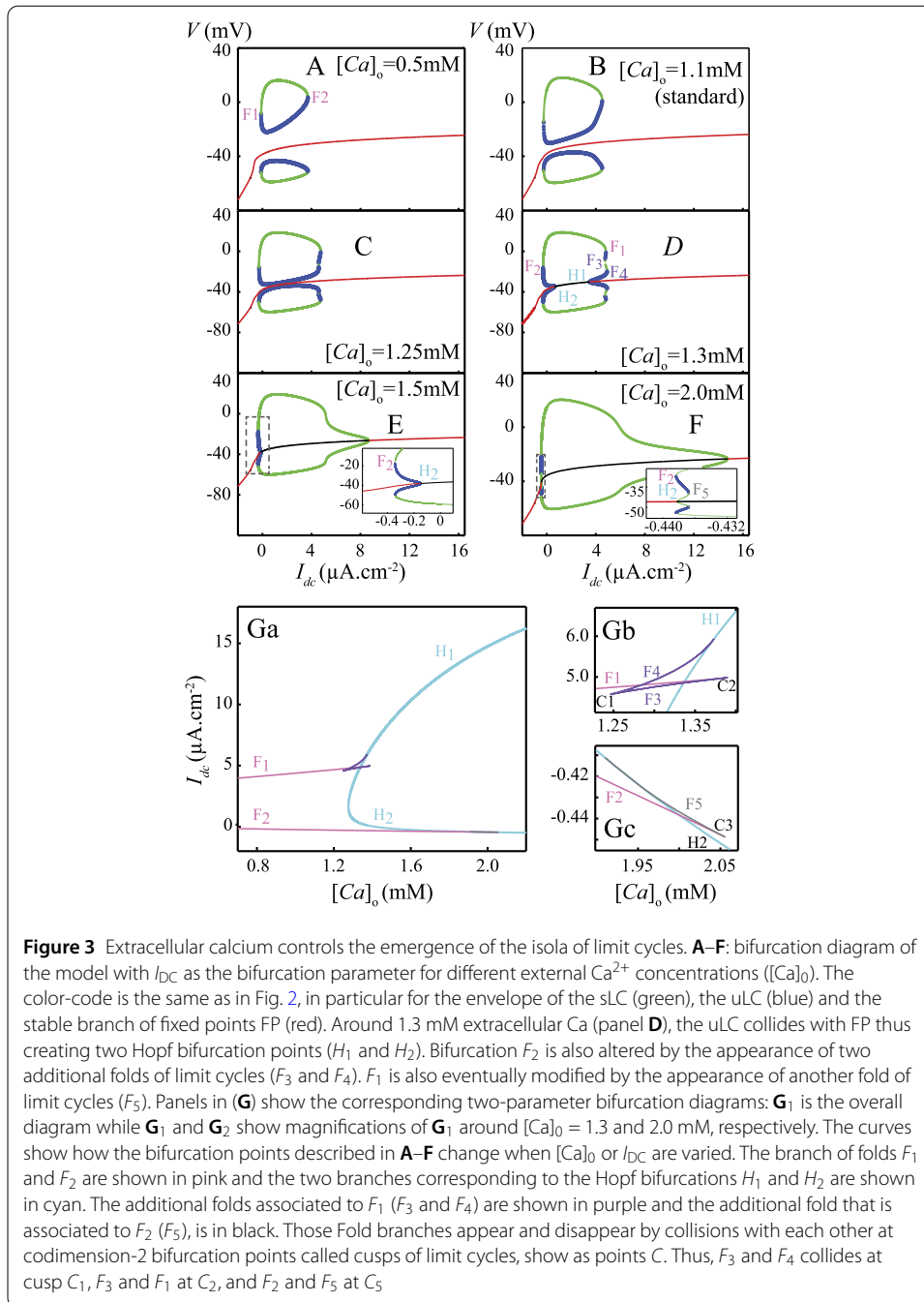
Bifurcation analysis provides an explanatory scheme for the emergence of the overall properties of a dynamical system (see e.g. [41] for an introduction). In bifurcation analysis of neuron models, the steady injected current (I_{DC} in our model) is the most important bifurcation parameter as it is used in experiments as a model of synaptic inputs to investigate the electric properties of the neuron. The power of this approach was first demonstrated by Rinzel and Ermentrout [41] who showed that the type I and II responses identified by Hodgkin [42] in crab neurons are due to different bifurcations (see Izhikevich [43] for a comprehensive exposure of the geometry of excitability of nerve cells). We therefore followed this approach and we built bifurcation diagrams of the model with I_{DC} as the bifurcation parameter.

In the presence of hyperpolarizing bias currents, the model has a unique stable attractor, the SD state (Fig. 2A). This state is actually stable in the global sense (i.e. with respect to any perturbation whatever its amplitude) since it is the only attractor in the phase space. Firing arises upon increasing the bias current I_{DC} to $I_{F_1} = -255.3 \text{ nAcm}^{-2}$, a value at which a unique neutrally stable periodic orbit appears (Fig. 2A). Two different branches of Limit Cycles (LC) emerge from this orbit: one of them (green) corresponds to stable LC (sLC) whereas the other one corresponds to unstable LC (uLC). This type of bifurcation is usually referred to as fold bifurcation of LC. The neutrally stable LC has a frequency of 17.8 Hz at the F_1 bifurcation point (Fig. 2B). These results suggest that the DCNn are type II neurons characterized by both a nonzero frequency and a nonzero spike amplitude at the bifurcation point [38]. Upon increasing I_{DC} , the amplitude of the sLC steeply increases while that of the uLC first decreases, exhibiting a minimum at $I_{\text{DC}} \simeq 1000 \text{ nAcm}^{-2}$ (inset Fig. 2A), and increases afterwards. Likewise, the amplitude of the sLC shows a maximum at $I_{\text{DC}} \simeq 1000 \text{ nAcm}^{-2}$ then decreases beyond this value. The parallel decrease of the amplitude of sLC and increase of the amplitude of uLC ultimately results in the merging of



the two LC branches into another neutrally stable LC through a second fold bifurcation at $I_{F_2} = 4256 \text{ nAcm}^{-2}$ (Fig. 2A). The theoretical maximum firing frequency of DCNn occurs at I_{F_2} and is 108 Hz, in the range of experimental maximum frequencies (80–120 Hz [7]). The branches of sLC and uLC thereby form a closed loop of limit cycles solutions of the model which is usually referred to as an isola of limit cycles (see e.g. Avitabile *et al.* [44] and Labouriau [45, 46] in the case of the HH model). This isola coexists with a branch of stable FP. Figure 2A thereby suggests that DCNn could switch between silent and firing modes of activity within the range of current $[I_{F_1}, I_{F_2}]$ in response to proper inputs. Spontaneous firing in the model disappears upon zeroing g_{NaV} (Fig. 2C). This result reproduces the finding that I_{Na} underlies the rising phase of the spike in the DCNn [4]. After g_{NaV} is zeroed, the membrane potential settles to a stable state with membrane potential $V = -44.4 \text{ mV}$, i.e. above the spike undershoot ($V_U = -58.1 \text{ mV}$). This result is at odds with properties of all neuron types studied so far (to the best of our knowledge) of which the membrane potential converges to values below V_U after blocking of the Na currents with TTX. Nevertheless, this model feature closely reproduces the experimental observation that, after blocking I_{NaV} with TTX, the DCNn settle to a depolarized stable voltage of $-42 \pm 2 \text{ mV}$ [4]. This property is well explained by the finding that I_{TCN} provides a depolarizing current to the membrane, as illustrated in Fig. 2D which shows that the branch of FP is shifted downright when I_{TCN} is blocked.

The report of a bistability between an isola of LC and a stable FP branch in a neuron membrane model is not unprecedented. Guttman *et al.* [12] have described similar dynamics in a model of the squid axon, which exhibits a stable point attractor coexisting with a stable firing mode of spikes when bathed in low $[Ca]_0$ solutions. This prompted us to investigate the hypothesis that $[Ca]_0$ may control bistability in DCNn by studying how $[Ca]_0$ affects the bifurcation diagram of the model (Fig. 3). With 0.5 mM external Ca^{2+} (Fig. 3A), the isola is characterized by the coexistence of a stable fixed point (red), an unstable limit

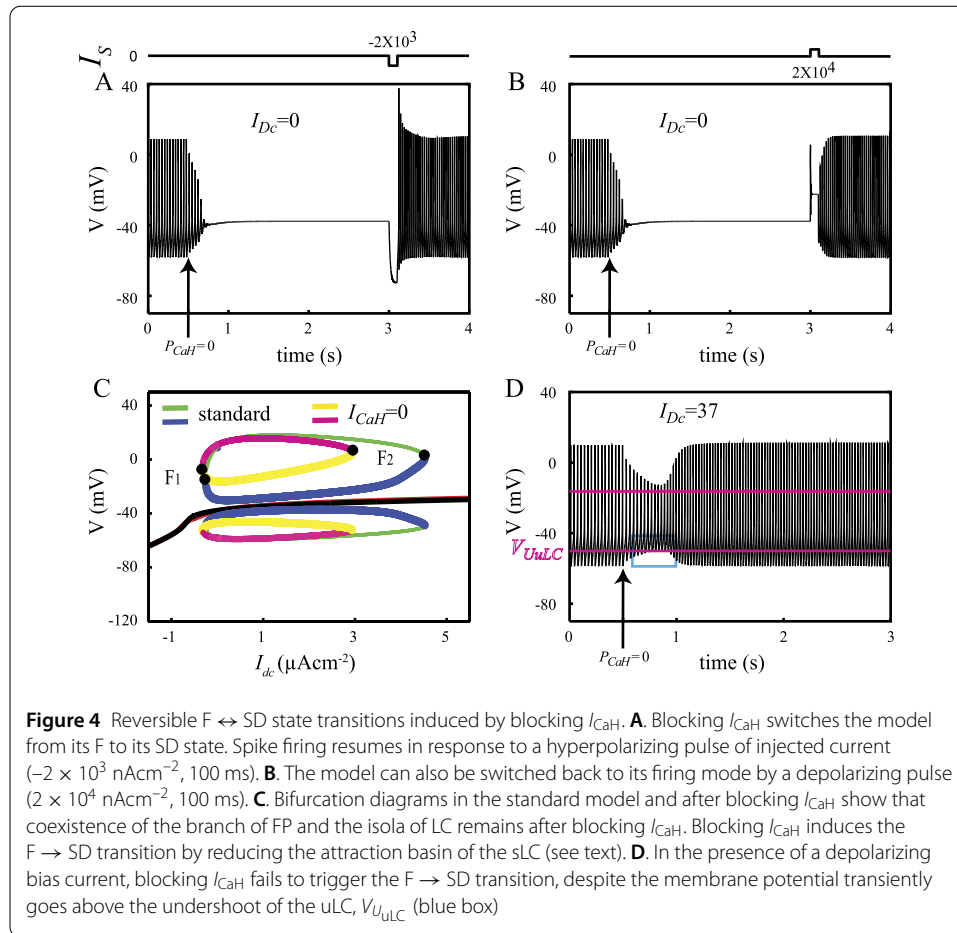


cycle (min-max values in blue) and a stable limit cycle (min-max values in green) within the range $I_{DC} = [0, 4] \mu A/cm^2$. Two folds of limit cycles (F_1 and F_2 , pink in Fig. 3G) locate the coalescence of the two limit cycles. With increasing external Ca^{2+} , the unstable limit cycle gets closer to the fixed point (Fig. 3B, C), colliding it for $[Ca]_0 \simeq 1.26$ mM (Fig. 3C). The collision with the fixed point gives birth to (Fig. 3G₁) two subcritical Hopf bifurcations (H_1 and H_2 , blue in G) between which the fixed point becomes unstable (black in D). In addition, a pair of limit cycles (one stable, one unstable) appears by a cusp of LC (C_1 in Fig. 3G₂), thus giving rise to two new folds of LC (F_3 and F_4 , purple in Fig. 3G₂). F_4 disappears by coalescence with H_1 and F_3 with F_1 in the cusp of limit cycles C_2 (Fig. 3G₂),

leaving H_1 as the only bifurcation point in the zone for $[Ca]_0 > 1.4$ mM (Fig. 3E). At even larger $[Ca]_0$ (around 2 mM), a new stable LC appears close to F_2 and H_2 as a result of H_2 becoming supercritical, giving rise to F_5 (Fig. 3F, gray in Fig. 3G₃). F_2 and F_5 in turn disappear by coalescence at the cusp of limit cycles C_3 (Fig. 3G₃), leaving H_2 as the only bifurcation point in the zone for $[Ca]_0 > 2.1$ mM (Fig. 3G₁). These results therefore suggest the existence of a bistability (stable fixed point SD + stable limit cycle sLC) at physiological $[Ca]_0$ in the electro-responsiveness of DCNn.

3.3 Reversible F ↔ DB transitions induced by blocking I_{CaH} : role of the separatrix between the F and SD states

Raman *et al.* [4] report that blocking Ca currents of DCNn switches their spontaneously firing activity to a silent depolarized mode at -37 mV. Our model reproduces this experimental result as it switches onto a silent depolarized state (SD) after blocking both of its Ca currents, I_{CaH} and I_{CaT} (not illustrated). The membrane voltage adopted by our model (-38 mV) is very close to the experimental value reported by Raman *et al.* [4]. The experimental protocol of Raman *et al.* prevented them to determine whether the $F \rightarrow SD$ switch results from blocking both Ca currents or from blocking only one of them because they blocked both currents with 2 mM cobalt (see [47]). We could readily address this question with the model. Blocking I_{CaT} (i.e. setting $P_{CaT} = 0$) does not induce a $F \rightarrow SD$ transition (result not shown). This finding is not surprising since I_{CaT} is almost completely inactivated at the spikes undershoot voltage ($h_{CaT} \simeq 5.5 \times 10^{-4}$), which is the more negative V value spontaneously reached by the model in its F mode. On the opposite, blocking I_{CaH} induces a $F \rightarrow SD$ transition (Fig. 4A). Following this switch, brief pulses of hyper- (Fig. 4A) or depolarizing (Fig. 4B) injected current reset firing in the model. Figure 4C explains this finding by showing that both the branch of FP and the isola of LC of the standard model are preserved after blocking I_{CaH} , thereby allowing theoretical $F \leftrightarrow SD$ state transitions. We now give evidence that the mechanism of the $F \rightarrow SD$ transition induced by blocking I_{CaH} finds its origin in the modifications of the shape of the isola of LC illustrated in Fig. 4C. Recall from Sect. 1 that the SD state is only locally stable. It therefore has a basin of attraction that is the set of initial conditions from which the model converges onto the SD state. However, in the bistable regime the coexisting sLC also has its own basin of attraction. Cooley *et al.* [8] early conjectured that for membrane models with only two variables, this situation implicates the existence of an uLC separating the basins of attraction of the two stable states. In other words, the separatrix between the basins of attraction of the SD and the F states in two-dimensional models is the orbit of the uLC in the phase plane. In $n > 2$ dimension models the separatrix must be a manifold of higher dimension than the one-dimensional uLC since the separatrix partitions the phase space into two attraction basins. Guttman *et al.* [12] have hypothesized that the separatrix contains the uLC and it is reasonable to suppose that it is a $n - 1$ dimension manifold. To our knowledge, neither of these two conjectures have been proved until now. Assuming that they are true (see the appendix), we propose that blocking I_{CaH} in our six-dimensional model triggers the $F \rightarrow DB$ transition by reducing the maximum amplitude of the uLC (compare blue and yellow undershoot voltages of the uLC in Fig. 4C). This shrinks the attraction basin of the sLC at such point that a trajectory located in the basin of attraction of the sLC before blocking I_{CaH} finds itself on the other side of the separatrix (inside the basin of attraction of the FP) when I_{CaH} is blocked and eventually converge to the SD state.



When a small tonic current ($I_{DC} = 37 \text{ nAcm}^{-2}$) is injected, blocking I_{CaH} is no more able to trigger the $F \rightarrow SD$ transition although the membrane voltage crosses several times the undershoot voltage of the uLC (Fig. 4D). This confirms that the separatrix between the F and SD attraction basins does not reduce to the uLC and is rather a manifold of larger dimension. We provide further evidence for this conjecture and that of Guttman *et al.* [12] in the Appendix. Taken together these results suggest that the coexistence of a branch of stable silent states with an isola of LC in the DCNn does not rest on the expression of Ca currents by the DCNn. I_{KCa} cannot play a central role in these dynamical features since it is almost completely inactivated at the low $[Ca]$ level reached by the model when the Ca currents are blocked ($m_{KCa} \simeq 10^{-3}$ at $[Ca] \simeq 50 \text{ nM}$). The origin of the peculiar bifurcation diagram of the standard model illustrated in Fig. 2A has therefore to be searched in the interactions between the remaining active currents in the model, namely I_{Na} , I_{Kdr} and I_{TCN} . This question is addressed after the following section, in which we expose the role played by I_{CaT} in the $F \rightarrow SD$ transitions triggered by hyperpolarizing current pulses in the standard model.

3.4 A mechanism for $F \rightarrow SD$ transitions triggered by current injections: the role of I_{CaT}

Figure 5A₁ (reproducing Fig. 1A₁ above) recalls that large hyperpolarizing current pulses can trigger a $F \rightarrow SD$ transition in the model. However, Fig. 5A₂ shows that the same cur-

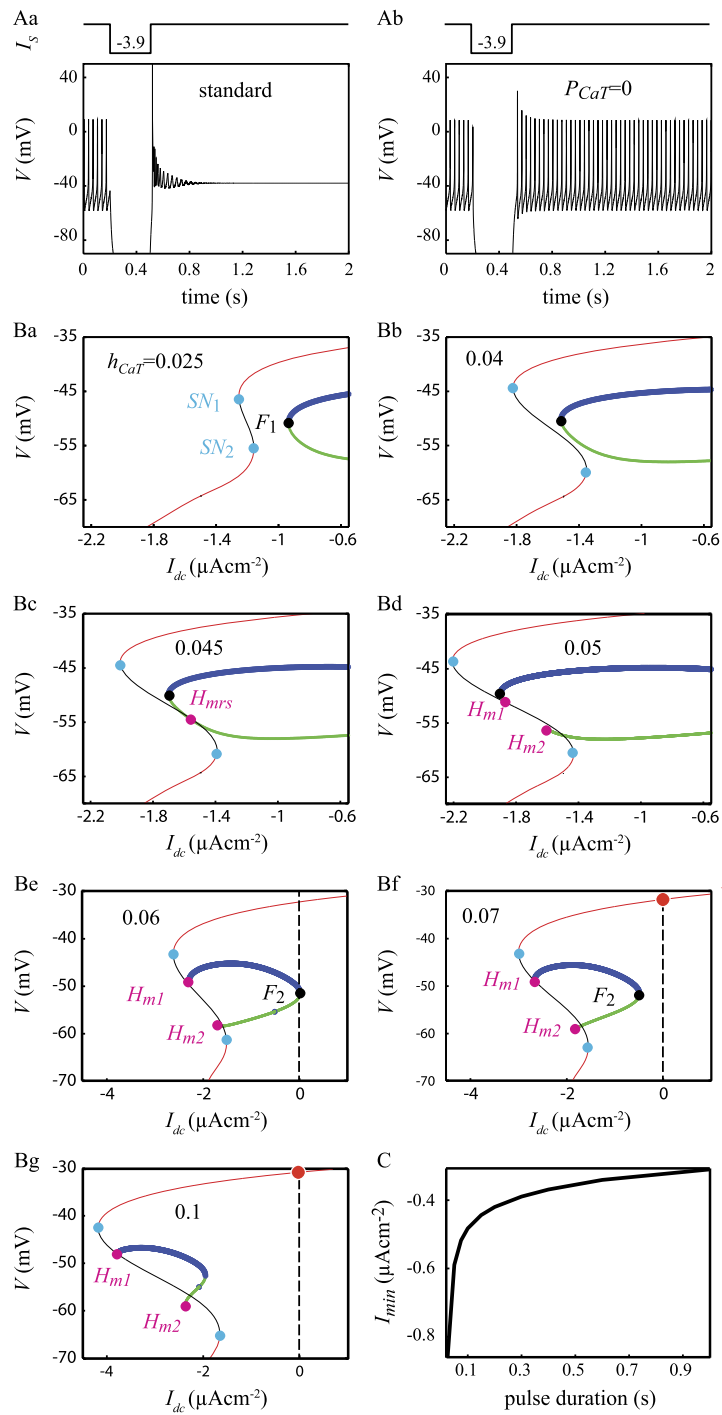
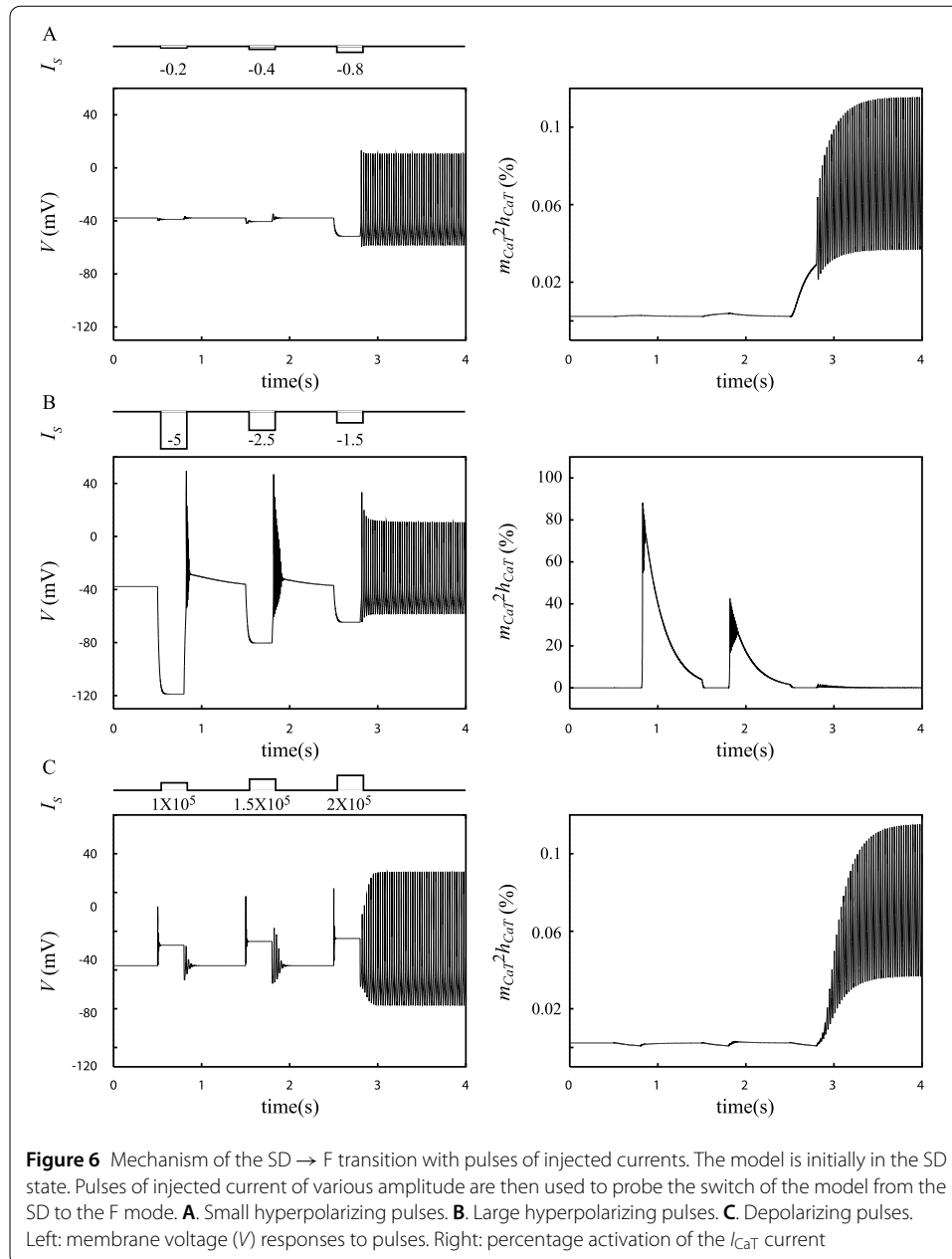


Figure 5 Contribution of I_{CaT} to $F \rightarrow$ SD transitions triggered by hyperpolarizing current pulses. **A.** Response of the standard model to a 300 ms hyperpolarizing pulse ($-3.9 \mu\text{Acm}^{-2}$) before (**A₁**) and after (**A₂**) blocking I_{CaT} . **B.** Evolution of the bifurcation diagram of a variant model where the inactivation variable h_{CaT} is considered an adjustable parameter. **C.** Minimum amplitude of a hyperpolarizing current pulse capable to trigger the $F \rightarrow$ SD transition as a function of the pulse duration

rent pulse fails to induce this transition if I_{CaT} is blocked. This result evidences the crucial role played by I_{CaT} in deciding whether a hyperpolarizing input can trigger a $F \rightarrow SD$ transition. Understanding the impact of I_{CaT} was complicated by the fact that both the steady-state value h_{CaT}^∞ and the time constant $\tau_{h_{CaT}}$ of the inactivation variable h_{CaT} of I_{CaT} are voltage-dependent so that both the magnitude and the duration of the current pulses determine the amount of recruited I_{CaT} (see Eq. (12)). We first investigated whether long duration current pulses (i.e. of duration $\gg \tau_{h_{CaT}}$) are able to trigger a $F \rightarrow SD$ transition in a variant model in which h_{CaT} is no longer a function of time and membrane voltage but a constant value freely adjustable in the $[0, 1]$ continuous interval. With $h_{CaT} = 0$, the bifurcation diagram of this variant model is nearly identical to that of the standard model (not illustrated). Increasing h_{CaT} to 0.025 induces a loss of stability of the FP branch with the appearance of two saddle-node bifurcations, SN_1 and SN_2 (Fig. 5Ba). The FP branch is stable below I_{SN_1} and above I_{SN_2} . The model is hence bistable for $I_{DC} \in [I_{SN_1}, I_{SN_2}]$, the unstable intermediate branch of FP points (black in Fig. 5B₁) delimiting the attraction basins of the two stable FP states. The gap between the two saddle-node bifurcations widens when h_{CaT} is increased (Fig. 5B₂). In addition, the F_1 limit of the isola of LC is shifted leftward so that $I_{F_1} \in [I_{SN_1}, I_{SN_2}]$: the model becomes tristable in this range of injected currents (two stable silent FP states and a stable LC). Both modifications of the bifurcation diagram go on as h_{CaT} is further increased up to 0.045 where the branch of uLC collides the unstable branch of FP points resulting in a homoclinic bifurcation of uLCs (Fig. 5B₃). Above this h_{CaT} value, another bifurcation occurs with the homoclinic bifurcation splitting into two homoclinic bifurcations, H_{m1} and H_{m2} (see Fig. 5B₄ for $h_{CaT} = 0.05$). Both bifurcations correspond to the collision of homoclinic orbits (corresponding to uLCs with a frequency equal to zero) with the unstable branch of FP. But as h_{CaT} keeps increasing, the F_1 limit of the isola keeps shifting to the left and the H_{m1} bifurcation turns into a homoclinic bifurcation of sLC at saddle node (for $h_{CaT} = 0.07$, Fig. 5B₅). In parallel with these effects on the left-hand side of the isola, increasing h_{CaT} also shifts the F_2 bifurcation to the left (see the sequence of Fig. 5B₁₋₆). Above $h_{CaT} = 0.06$, $I_{F_2} < 0$ so that the only attractor remaining in the phase space for $I_{DC} = 0$ is the SD state (solid red circle in Fig. 5B₆₋₇) and the model is therefore forced to converge onto this SD state. We therefore conclude that hyperpolarizing current pulses trigger the $F \rightarrow DB$ transition because they de-inactivate I_{CaT} which leads to the disappearance of the isola of LC. In support of this conclusion, Fig. 5C shows that the minimum amplitude of a hyperpolarizing pulse to trigger the $F \rightarrow DB$ transition decreases with the pulse duration, in agreement with the fact that having longer duration pulses allows for recruiting larger fractions of I_{CaT} owing to the non-instantaneous activation of this current.

3.5 Mechanism of $SD \rightarrow F$ transitions triggered by current injections: crossing the separatrix

From a biological standpoint, the hypothesis of the existence of a silent depolarized state only holds if the DCNn in the SD state are one way or another capable to switch back to their F mode. Otherwise, the entire population of DCNn would eventually become trapped to the SD state. As this prediction contradicts observations of active DCNn in fully developed organisms, our model had (i) to provide evidence for physiological stimuli capable to trigger $SD \rightarrow F$ transitions and (ii) explain the mechanism of these transitions in order to sustain the hypothesis of the SD state in DCNn. Our standard model does



produce such SD \rightarrow F transitions when hyperpolarizing (Fig. 1D₁) or depolarizing pulses (Fig. 1D₂) are injected. We next studied the mechanism of this transition.

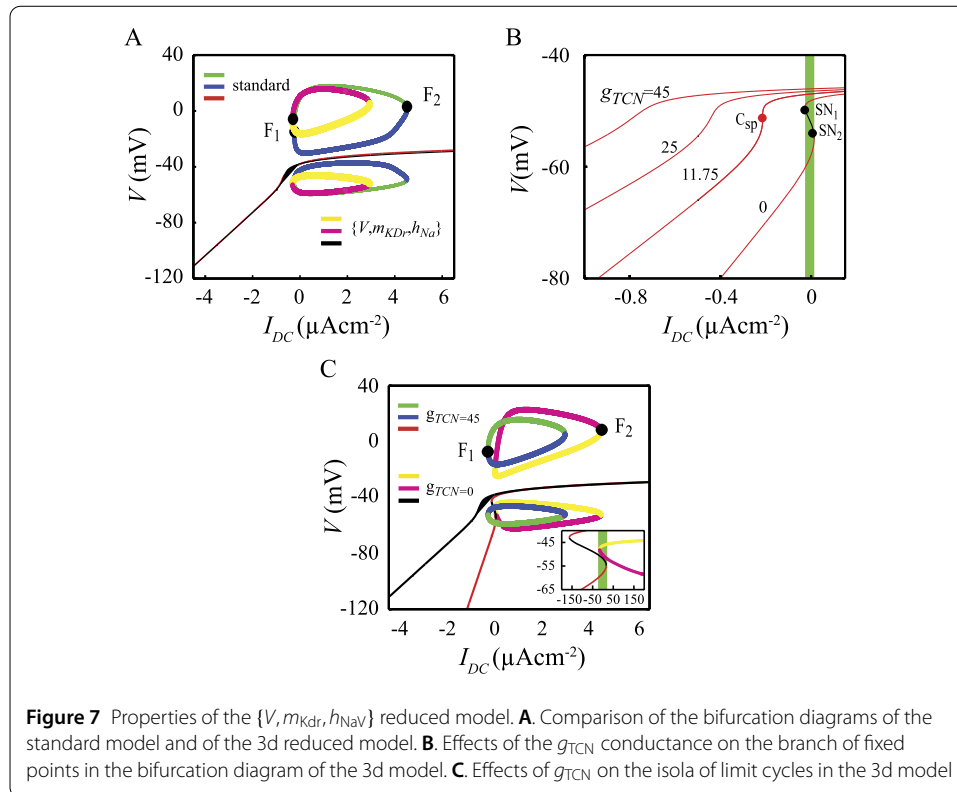
Figure 6A shows that a hyperpolarizing pulse must have a minimum amplitude in order to trigger a SD \rightarrow F transition. However, this minimum amplitude is clearly not a simple threshold value since Fig. 6B shows that if its amplitude is too large, a hyperpolarizing pulse fails to trigger the switch because it de-inactivates I_{CaT} (Fig. 6B, the first two pulses are large enough to activate 40 to 80% of this current). On the other hand, the mechanism of the SD \rightarrow F transition triggered by pulses of moderate amplitude like the third pulse in Fig. 6A cannot involve I_{CaT} . Indeed, this current remains inactivated during and after the pulse (<0.15% activation, Fig. 6A) so one does not expect significant changes in the bifurcation diagram due to I_{CaT} deactivation. In this case, the transition can only be explained by the

fact that hyperpolarizing pulses of moderate amplitude bring the trajectory of the model across the separatrix between the F and SD attraction basins. After entering the F state attraction basin, the model eventually converges to this state. Therefore, to trigger a SD \rightarrow F transition in the model, the amplitude of a hyperpolarizing pulse must be within an effective range: it must be large enough to drive the system on the other side of the F–SD separatrix but weak enough so as not to de-inactivate I_{CaT} .

A fundamental consequence of the above analysis is the prediction that any perturbation driving only once the trajectory across the separatrix should be able to trigger a SD \rightarrow F transition. The result illustrated in Fig. 6C confirms this prediction as it shows that not only hyperpolarizing currents but also depolarizing current pulses can trigger a SD \rightarrow F transition. Altogether, these results support the hypothesis that crossing the separatrix between the basins of attraction of the F and SD state is the basic mechanism by which phasic inputs, either depolarizing or hyperpolarizing, trigger a SD \rightarrow F state transition. As shown above, altering the calcium currents induces qualitative changes of the bifurcation structure (i.e. changes of the size of the basins of attraction or translations of the bifurcation points), but preserves the overall structure, i.e. the coexistence of a branch of stable silent states with an isola of limit cycles. Therefore, the origin of the peculiar bifurcation diagram of the standard model illustrated in Fig. 2A does not rest on the expression of Ca currents in the DCNn but has to be searched in the interactions between the remaining active currents in the model, namely I_{NaV} , I_{Kdr} and I_{TCN} .

3.6 The $\{V, m_{Kdr}, h_{NaV}\}$ sub-system and the role of I_{TCN} in stabilizing the SD state

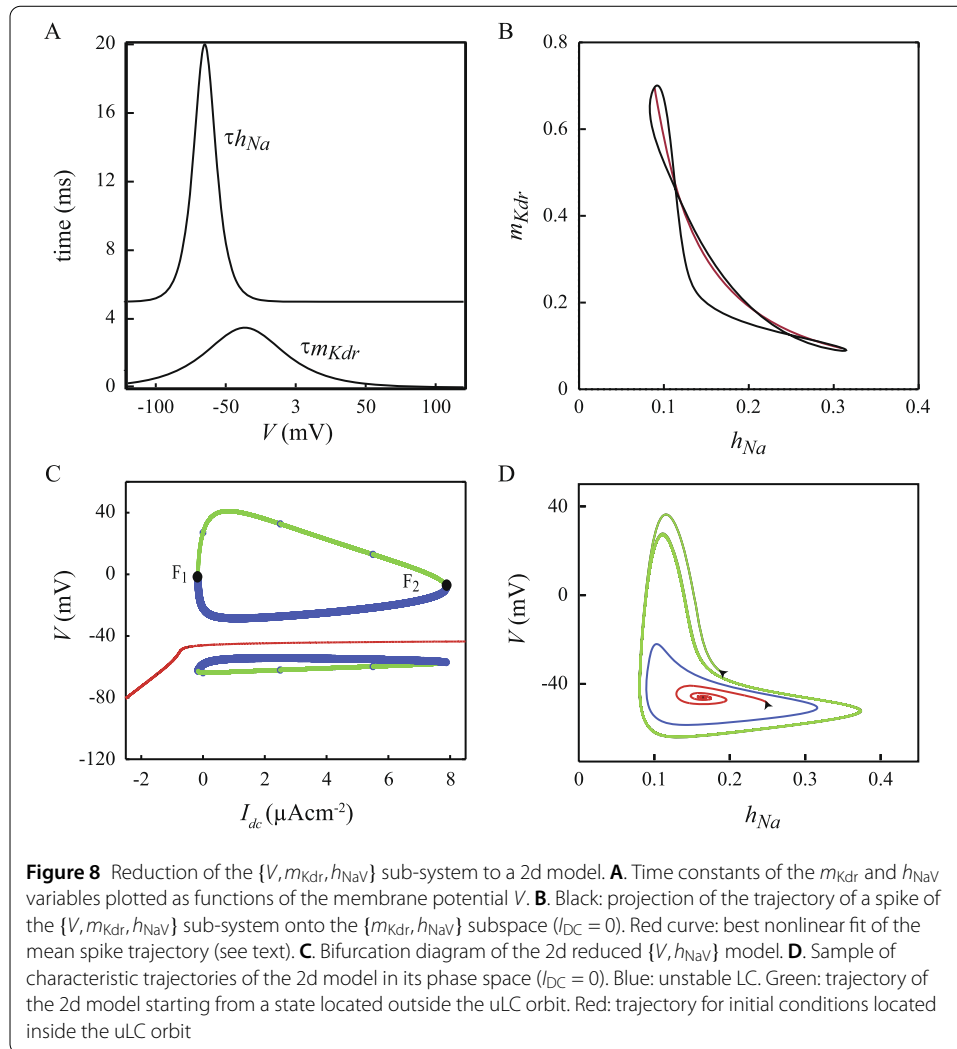
We next investigated how the interactions between I_{Na} , I_{Kdr} and I_{TCN} explain the coexistence of a branch of FP with an isola of LC in the DCNn. We have shown above that neither the Ca currents nor the Ca-dependent K currents are required to produce the basic bifurcation diagram of Fig. 2A. After withdrawing these currents, the standard model reduces to a simplified model with only three variables: the membrane potential V , the activation variable of I_{Kdr} , m_{Kdr} and the inactivation variable of I_{NaV} , h_{NaV} . We therefore refer to this reduced model as to the $\{V, m_{Kdr}, h_{NaV}\}$ sub-system. Figure 7A shows that this sub-system retains the basic dynamical features of the standard model. In particular, the FP branch is nearly identical in the two models. Moreover, the $\{V, m_{Kdr}, h_{NaV}\}$ sub-system also exhibits an isola of LC albeit in a narrower range of tonic currents. Simulations of the reduced model reveal that pulses of injected current can trigger reversible SD \leftrightarrow F like those described above in the full model (not illustrated). The FP branch exhibits a marked sensitivity to the magnitude of the g_{TCN} conductance. Reducing this parameter from its standard value ($45 \mu\text{Scm}^{-2}$) shifts to the right the entire branch of FP along the I_{DC} axis. This result stems from the value of the I_{TCN} reversal potential ($E_{TCN} = -34 \text{ mV}$) that defines this current as inward (depolarizing) for all points of the FP branch, since they all are below E_{TCN} . Hence, reducing g_{TCN} requires increasing the value of I_{DC} to achieve a FP with the same voltage. As g_{TCN} is reduced to $11.75 \mu\text{Scm}^{-2}$, the FP branch exhibits a point of infinite slope (red dot in Fig. 7B). This point corresponds to a cusp bifurcation. Below the cusp bifurcation, the FP branch is no longer stable for every I_{DC} value, but exhibits two saddle-node bifurcations (SN_1 and SN_2) that form a hysteresis loop (green rectangle in Fig. 7B) for the example of $g_{TCN} = 0$. Hence, the model has two coexisting stable silent modes of activity for values for g_{TCN} values below the cusp bifurcation. The isola of LC still exists in the $\{V, m_{Kdr}, h_{NaV}\}$ sub-system without I_{TCN} (Fig. 7C). But the



model has now three stable attractors, the sLC and the two stable points of the FP branch mentioned above. Appropriate stimuli can theoretically trigger transitions between these three modes of activity in the range of I_{DC} values delimited by green box in the inset of Fig. 7C. These results therefore suggest that the functional role of I_{TCN} in the DCNn is to stabilize the SD state over the entire range of tonic currents provided by the synaptic inputs.

3.7 Reduction of the model to 2D: evidence for a central role of I_{NaV} in setting the DCNn electric personality

The properties of the $\{V, m_{Kdr}, h_{NaV}\}$ reduced model suggest that the interactions between I_{NaV} and I_{Kdr} play a crucial role in the emergence of the basic bifurcation diagram of the standard model. However, this sub-system does not allow a deep understanding of these interactions owing to their nonlinear nature. This prompted us to search for an even stronger reduction of the standard model to two dimensions, i.e. the minimum dimension for the emergence of limit cycles in ODE systems. To achieve this goal, we followed the approach of Fitzhugh [48] and searched for a relation between m_{Kdr} and h_{NaV} along the trajectory of a spike in the model ([48, 49] and see Rinzel [50] and Gerstner *et al.* [31] for developments of Fitzhugh's mathematical approach on biophysical grounds). Fitzhugh observed that, in the squid axon, the projection of a spike trajectory in the (m_{Kdr}, Oh_{NaV}) plane is close to a straight line. This allowed one to lump together m_{Kdr} and h_{NaV} into a so-called recovery variable, w , exploiting their linear relation interdependence. Combined with the assumption of instantaneous equilibrium for m_{NaV} , this process allowed for the reduction of the original four-dimensional Hodgkin and Huxley model [16] to a simpler, two-dimensional model that keeps the fundamental dynamical features of the original

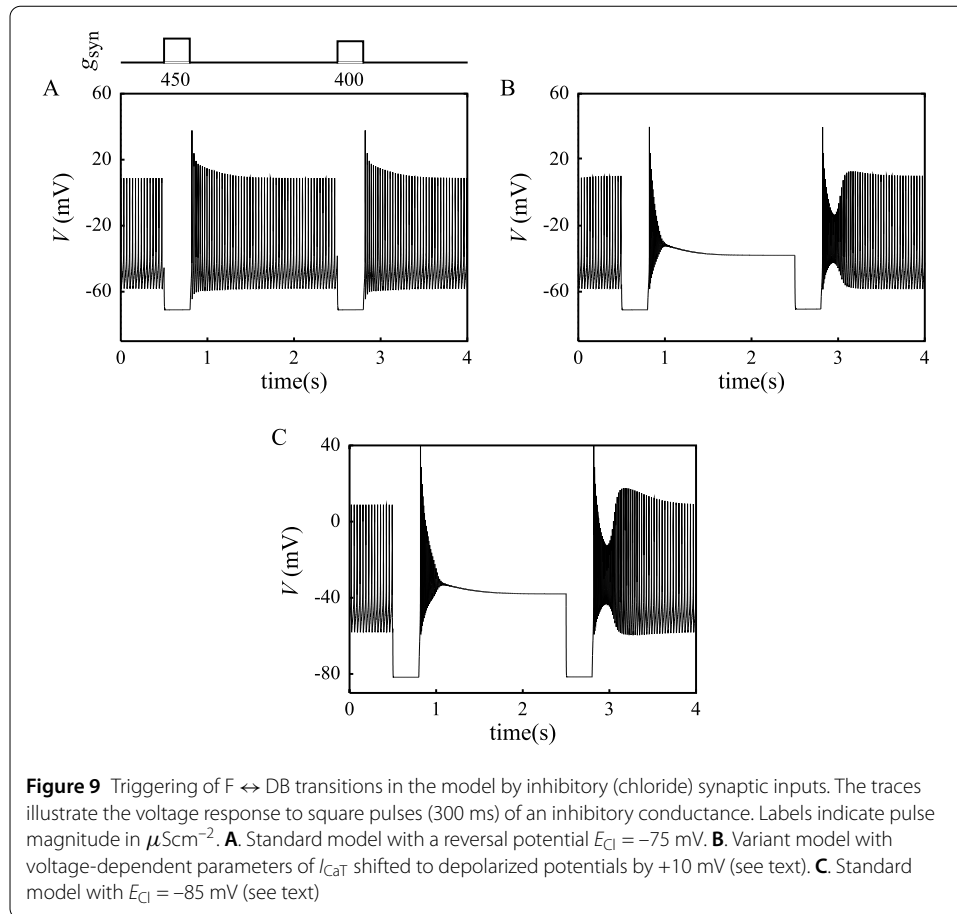


model. Nevertheless, the implementation of this method of reduction of dimensionality also requires an appropriate expression for the (voltage-dependent) time constant τ_w for the new variable w . The solution was simple in the squid axon because the voltage dependencies of $\tau_{m_{Kdr}}$ and $\tau_{h_{NaV}}$ have similar shapes so that the voltage dependency of τ_w can be set as a trade-off between that of $\tau_{m_{Kdr}}$ and $\tau_{h_{NaV}}$ (see Fig. 17, Chap. 2 in [22]). On the opposite, in our DCNn model, the magnitudes and voltage-dependent characteristics of $\tau_{m_{Kdr}}$ and $\tau_{h_{NaV}}$ are too different to be reconciled by a single, trade-off behavior model for τ_w (Fig. 8A). We therefore turned to another approach and built 2d models that preserve either $\tau_{m_{Kdr}}$ or $\tau_{h_{NaV}}$. In our model the trajectory of a spike in the $\{V, m_{Kdr}, h_{NaV}\}$ model projected into the (m_{Kdr}, h_{NaV}) plane is not a simple curve (Fig. 8B). Like the projected curve of the Hodgkin–Huxley model, it exhibits two double points (see Fig. 6 in [49]) and we therefore searched for the best nonlinear fit of the trajectory in the (m_{Kdr}, h_{NaV}) plane. Firstly, we built a 2d model preserving the properties of I_{Kdr} by fitting the h_{NaV} versus m_{Kdr} relation. We found that the power law $h_{NaV} = 0.07/m_{Kdr}^{0.65}$ provides a good fit of the mean trajectory of a spike in the (m_{Kdr}, h_{NaV}) plane (not illustrated). By substituting this expression for h_{NaV} into the I_{NaV} equation we obtained a first 2d reduced model, the $\{V, m_{Kdr}\}$ sub-system, that comprises a unique voltage-dependent time constant $\tau_{m_{Kdr}}$.

However, this model fails to capture the features of the $\{V, m_{Kdr}, h_{NaV}\}$ model given that it fails to produce repetitive firing (not illustrated). We therefore turned to the alternative and fitted the m_{Kdr} versus h_{NaV} relation. We found that this relation is well fitted by the equation $m_{Kdr} = 0.0145/h_{NaV}^{1.6}$. After substituting m_{Kdr} by this equation into the I_{Kdr} current equation, one obtains a second 2d reduced model, the $\{V, h_{NaV}\}$ sub-system. Like the $\{V, m_{Kdr}\}$ sub-system, it contains a unique voltage-dependent time constant but it is τ_{hNa} instead of τ_{mKdr} . Figure 8C shows that the $\{V, h_{Na}\}$ sub-system retains the qualitative dynamical features of the $\{V, m_{Kdr}, h_{NaV}\}$ model with an isola of LC coexisting with a branch of stable FP. The global properties of the $\{V, h_{NaV}\}$ sub-system can be understood geometrically since the model is 2d. Figure 8D depicts characteristic trajectories of the model for $I_{DC} = 0$. The blue closed curve is the trajectory of the uLC corresponding to $I_{DC} = 0$ in the bifurcation diagram. We found that any trajectory starting from an initial condition located inside the region bounded by the blue curve converges onto the FP point (see for example the red trajectory in Fig. 8D). On the opposite any trajectory starting outside the region defined by the blue curve converges onto the corresponding sLC in the bifurcation diagram (see for instance the green trajectory in Fig. 8D). We conclude that the blue curve is the separatrix between the attraction basins of the FP and of the sLC. Moreover, we observed that the $\{V, h_{NaV}\}$ sub-system loses the characteristic features of the $\{V, m_{Kdr}, h_{NaV}\}$ reduced model if τ_{mKdr} rather than τ_{hNaV} is used in the I_{NaV} equation: the isola of LC disappears whereas the FP branch remains unaffected. This shows that the characteristics of the voltage-dependent time of inactivation of I_{NaV} are also fundamental for the coexistence of an isola of LC and of a branch of FP. Together these results suggest that the most important current for these dynamical features is I_{NaV} .

3.8 The triggering of reversible F ↔ SD transitions by synaptic inputs

From a functional standpoint, it is crucial to determine whether F ↔ SD transitions in DCNn actually occur in response to synaptic inputs provided by MF and PC. Indeed, the ideal phasic current sources used in previous sections have an infinite resistance whereas synaptic currents have a nonzero conductance that may prevent state transitions to occur by shunting the neuron membrane. Moreover, synaptic currents have an inversion potential which sets limits to voltage changes that can be triggered by activating these conductances. We therefore investigated this question with a variant model in which ideal phasic currents were replaced by models of synaptic currents, i.e. current sources having a nonzero conductance and an inversion potential: $I_{syn} = g_{syn}(V - E_{syn})$. Experiments estimate the Nernst potential of Cl^- ions in DCNn to be $E_{Cl} = -75$ mV [3, 51]. Figure 9A illustrates the response of the standard model to a pair of successive pulses of synaptic current that model the inhibitory inputs of PC synapses onto the DCNn. Both pulses (of different amplitudes) interrupt the tonic firing of spikes in the model in agreement with experimental observations that PC inputs can silence DCNn [51]. After the pulse, the DCNn, however, resumes firing spikes after a ~300 ms period of increased firing frequency. We found that such synaptic inhibitory pulses cannot trigger a F → DB transition in those conditions, whatever the duration or amplitude of the pulse (data not shown). Examination of I_{CaT} dynamics during the pulse showed that inhibitory synaptic conductances deactivate a smaller amount of I_{CaT} compared to direct current injections, thus explaining the absence of F → SD transition by inhibitory synaptic conductances. These results may lead one to conclude that physiological inputs from PC are unable to trigger F → SD transitions in DCNn. However, Boehme *et al.* [52] have observed that large synaptic inhibition



of DCNn by Purkinje cells potentially elicit rebound potentials that are underlain by I_{CaT} . These authors suggested that these observations could result from an erroneous estimate of either the voltage dependence of I_{CaT} or the value of the chloride Nernst potential E_{Cl} . They noticed that the previous estimates of the voltage characteristics of I_{CaT} have been derived from DCNn recordings made in the soma where the density of I_{CaT} is smaller than in the DCNn dendrites [14]. Owing to difficulties to achieve perfect space-clamp of the membrane voltage over the entire neuron surface, these authors estimated that the actual voltage-dependent parameters of I_{CaT} could be less negative by as much as 10 mV. Figure 9B illustrates the model response to the same stimulation protocol as Fig. 9A but after a +10 mV shift of the voltage-dependence of I_{CaT} . The first current pulse now is able to trigger a $F \rightarrow SD$ transition while the second pulse induces the opposite transition, switching back the model to its F state. Boehme *et al.* [52] further suggested that E_{Cl} in the DCNn may also be wrongly estimated by whole cell recordings since the patch pipette imposes its electrolytes composition to the recorded neuron. They estimated that the physiological E_{Cl} could be more negative, down to -85 mV. This negative shift of E_{Cl} induces effects that are qualitatively identical to positive shifts of the I_{CaT} voltage-dependency (Fig. 9C), the first pulse triggering a $F \rightarrow SD$ transition and the second pulse resetting the neuron to its firing state.

4 Discussion

The mathematical model presented in this study sketches an original electric personality for the neurons of the deep cerebellar nuclei (DCNn) which remained unsuspected until now in spite of experimental data evidencing puzzling state transitions in these neurons. The pioneer investigation of DCNn intrinsic electric properties by Jahnsen ([2] and [51]) reported that spontaneously active DCNn can be switched to a silent state and back to their firing mode by pulses of injected current (Fig. 5 in [2]). Jahnsen referred to the silent state as a 'steady depolarization and inactivation of the spikes' and our terming 'SD state' stands as a shortcut for this description. The study of Raman *et al.* [4] subsequently reported strikingly similar results with patch-clamp recordings showing that depolarizing current pulses can switch DCNn up to a silent depolarized state until the membrane is actively hyperpolarized by a current injection. Notice that the calling of this state a 'depolarization block' (DB) by Raman *et al.* [4] actually appears misleading. Indeed, many (if not all) neurons exhibit an inactivation of their spike mechanism in response to large depolarizing currents which is called DB (see e.g. midbrain dopamine neurons [53], hippocampal CA1 pyramidal neurons [54] and layer 5 pyramidal neuron of rat's visual cortex [43]). However, the DB does not outlast the duration of its triggering depolarizing current in all cases that we are aware of, showing that the DB is not a self-sustained state. In order to highlight these differences, we have chosen to term lasting depolarizations of DCNn as a 'SD state', this acronym standing for a shortcut of properties of these lasting sustained depolarizations initially described by Jahnsen [2]. Experimental data of Jahnsen [2] and Raman *et al.* [4] therefore suggest that the SD state may be a genuine state of the DCNn distinct from their spontaneously firing regime (F mode). Since a previous model of DCNn intrinsic electrical properties did not reproduce the coexistence of distinct firing regimes [7], we have built a new model to investigate the hypothesis of a stable depolarizing state in the DCNn, its relation with the spontaneous firing state and interactions between membrane ion currents that give rise to the coexistence of these two states.

Our model uses the latest experimental findings on active membrane ion currents in DCNn to suggest that DCNn have two coexisting stable electrical states. One them is the F mode in which neurons fire fast spikes at low spontaneous frequencies in agreement with *in vitro* studies [2–7]. The other state is a silent mode of activity characterized by a depolarized membrane potential at around -38 mV. We call it the SD state (for stable depolarized state) to stress the proposition that it is locally stable and excitable according to our model. This is evidenced by the fact that our model can be switched back and forth between its SD and F modes by brief pulses of de- or hyperpolarizing currents (see Fig. 1). According to our results (Fig. 2), these bistability properties of the DCNn may reflect the fact that these neurons lay at rest between two-fold bifurcations delimiting an isola of limit cycles which coexists with a branch of stable fixed points. The FP for $I_{DC} = 0$ would correspond to the plateau depolarization reported by Jahnsen [2] and by Raman *et al.* [4]. To our knowledge, such dynamical properties have been previously described only in the squid axon bathed in low $[Ca]_0$ saline [12].

Our model is a single-compartment, isopotential simplification of a cell that actually exhibits a more complex morphology with dendrites and soma. This simplification is in part justified by previous modeling studies of the passive properties of these cells that suggest that these cells are moderately electrotonically compact [7]. A first extension of our model consists in lumping the whole dendritic tree into a unique effective isopotential

compartment and connecting it to our initial soma model with a coupling conductance. Preliminary investigation of the resulting two-compartment system suggests that the capacitive and passive resistance loads imposed by the dendritic compartment to the soma are unlikely to challenge the basic mechanism that we propose to explain the transitions from the firing to the SD state in DCNn. In fact, the documented enrichment of DCNn dendrites in CaT current (14) could even boost the facility with which hyperpolarizing inputs can trigger these transitions.

4.1 Experimental testing of the model predictions

Our analysis of the mechanisms underlying $F \leftrightarrow SD$ transitions with the standard version of the model and variant versions mimicking pharmacological block of the different membrane ion currents suggests three experiments to unambiguously test the hypothesis of F–SD states bistability in the DCNn. These experiments could be achieved with standard intracellular recording of DCNn in cerebellum slices. *Experiment I—evidence for a branch of SD states*: our model predicts that recorded DCNn should reach a silent state of activity upon injecting them with sufficiently large amounts of steady depolarizing currents. Notice that this behavior is expected for any neuron type whose rising phase of the spike is underlain by a voltage-dependent Na current exhibiting inactivation. Unlike other neurons however, our model predicts that a DCNn should remain in this silent state when the amplitude of injected currents is decreased back at a rate sufficiently slow to prevent crossing of the separatrix between the F and SD states. Then, starting from hyperpolarized membrane potentials, our model predicts that the recorded DCNn should remain silent when the magnitude of the hyperpolarizing current is slowly reduced down to zero and even upon injecting large depolarizing currents. *Experiment II—evidence for an isola of limit cycles*: this second experiment investigates the firing mode of the DCNn with the help of standard (firing frequency vs I_{DC}) curves. Injecting depolarizing steady currents of growing magnitude into spontaneously active DCNn should increase their firing frequency up to a maximum current value (I_{F2} in Fig. 1) beyond which the DCNn should switch to a silent state. Conversely, in a spontaneously firing DCNn, increasing the magnitude of the tonic hyperpolarizing current above I_{F1} should abruptly switch the neuron to its silent mode. The observation of this result would lead one to categorize the DCNn as type II neurons according to the Hodgkin classification [42]. The latter part of this experiment should especially be achieved in the presence of broad-spectrum inhibitors of post-synaptic channels to remove spontaneous synaptic activity in slices. Membrane potential fluctuations due to ongoing synaptic activity would hinder determining if the DCNn minimal firing frequency is actually nonzero. *Experiment III—changing the external Ca^{2+} concentration*: this experiment tests the model prediction that the DCNn can be made to adopt the classical bifurcation scenario for type II neurons, by turning the left-hand side fold bifurcation of the isola into a subcritical Hopf bifurcation and the right one into a supercritical Hopf bifurcation (see [43]) by increasing $[Ca]_0$. These changes of bifurcation would not be accompanied by qualitative modification of the f/I relationship. But they could be identified by a continuous decrease of the spike amplitude down to zero upon increasing the driving current up to the right-hand side bifurcation. *Experiment IV—extent of I_{Na} inactivation in the SD state*: intracellular recordings could (i) check that I_{Na} is not fully inactivated in the SD state and (ii) investigate whether the full blockage of I_{Na} with TTX prevents DCNn state transitions by removing the SD state.

4.2 Ionic currents and dynamics of the model

The analysis of the standard model and its lower dimension variants suggest that the voltage-dependent properties of Na currents are of paramount importance in the state transitions displayed by the DCNn *in vitro*. In order to justify this major conclusion, we come back to the biophysical foundations of our model, namely the set of ion currents extracted from the experimental literature on the DCNn to build our model and their mathematical formulation. To avoid introducing unjustified hypotheses, we assumed that voltage-dependent currents obey the classical Hodgkin–Huxley formalism which has proven capable to reproduce the qualitative dynamics of most neuron types studied so far with mere parameter adjustments. For $I_{K_{dr}}$ this hypothesis is consistent with the finding by Raman *et al.* [4] of a classical delayed rectifier K current in DCNn. However, the large time constant of activation reported in this study (12 ms at +12 mV) suggests that this voltage-dependent current is carried by (slow) Kv2 channels (see e.g. [29]) whereas other studies give no evidence for the expression of Kv2 channels by DCNn. These studies rather show that DCNn express (fast) Kv3 channels and that these channels are functional (see Methods). Our model was accordingly designed with a voltage-dependent time constant for $I_{K_{dr}}$ corresponding to fast Kv channels. Nevertheless, we investigated the possible involvement of Kv2 channels in the DCNn electro-responsiveness with a variant model comprising a slowly activating K current, $I_{K_{drS}}$, in addition to $I_{K_{dr}}$. $I_{K_{drS}}$ was given the same voltage-dependence as $I_{K_{dr}}$ but its time constant was multiplied by 11 to achieve a value of 12 ms at +12 mV. Adding $I_{K_{drS}}$ to the model with the same conductance as $I_{K_{dr}}$ did not change the overall structure of the model's bifurcation diagram (compare panels A and B in Fig. 10). However, it increased the width of the isola of LCs and reduced the spontaneous firing frequency from 28.9 Hz to 25.5 Hz. This frequency could even be reduced to 20 Hz (the spontaneous firing frequency of DCNn *in vitro* [2–7]) by increasing the $g_{K_{drS}}$ value to 3.3 times that of $g_{K_{dr}}$ (not illustrated). These results suggested that previous studies of Kv channels in DCNn may have missed the Kv2 channels implied by the results of Raman *et al.* [4] and that currents through Kv2 channels underlie the low spontaneous frequency firing of DCNn. To address this hypothesis, we fixed the value of $g_{K_{drS}}$ and decreased that of $g_{K_{dr}}$ to determine to what extent slow Kv3 channels are mandatory to explain the observed firing dynamics of DCNn. Decreasing $g_{K_{dr}}$ diminishes the width of the isola of LC down to $g_{K_{dr}} = 3 \times 10^3 \mu\text{Scm}^{-2}$, where the branch of SD states loses its stability (Fig. 10C check). Nevertheless, overall stability of the FP branch was restored by increasing the conductance of I_{TCN} to $3 \times 10^3 \mu\text{Scm}^{-2}$, suggesting that the functional role of I_{TCN} is to stabilize the SD state of DCNn. We tested this proposal by reducing $g_{K_{dr}}$ down to the complete withdrawal of the fast K_V current in the model. The range of tonic currents over which the FP branch is unstable in the hybrid K_{drs} – K_{dr} variant model (Fig. 10B) was even more enlarged after switching the $I_{K_{dr}}$ model to solve Kv2-like dynamics (Fig. 10E). Nevertheless, increasing g_{TCN} proved again capable to resolve this issue as shown by panel F in Fig. 10 displaying the bifurcation diagram of the model endowed with g_{TCN} to $215 \mu\text{Scm}^{-2}$. Beyond strengthening our proposal on the functional role of I_{TCN} , these results demonstrate that the basic bifurcation scenario of the standard model can be achieved by a model comprising only slow Kv channels.

Adequacy of the classical HH formalism to model voltage-dependent Na currents in DCNn proved more challenging owing to two reasons: (i) the integer power to which raise variable m_{NaV} and (ii) the evidence for a resurgent Na current in DCNn (Ref) not

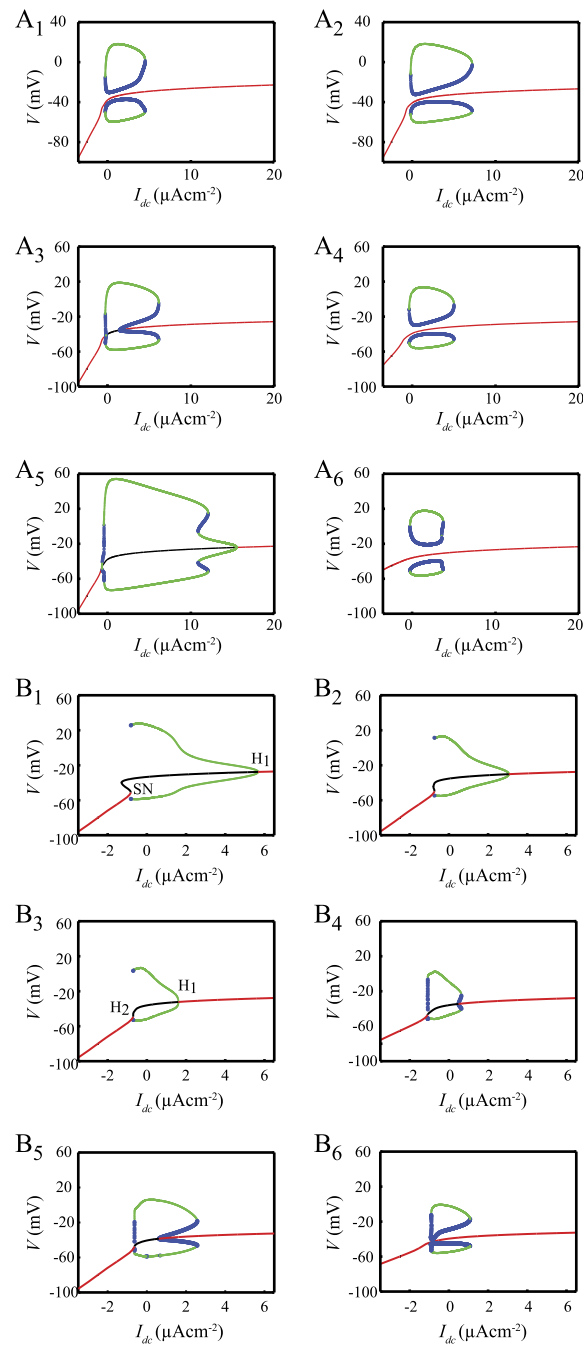


Figure 10 Robustness of the model's bifurcation diagram to parameters-models of I_{Kdr} and I_{Nav} (see text). **A.** Impact of putative Kv2 channels. Symbol I_{KdrS} stand for the standard I_{Kdr} after its voltage-dependent time constant was scaled up to model (slow) Kv2 channels. **A₁**. Standard model. **A₂**. After addition of I_{KdrS} (with the same conductance as I_{Kdr}). **A₃**. Same as **A₂** with g_{Na} decreased to $3000 \mu S cm^{-2}$. **A₄**. Same as **A₃** with g_{TCN} increased to $75 \mu S cm^{-2}$. **A₅**. With I_{KdrS} as the sole voltage-dependent K current (model's standard conductance value). **A₆**. Same as **A₅** with $g_{TCN} = 215 \mu S cm^{-2}$. **B.** Impact of the persistent component of I_{Nav} identified in DCNn. Symbol I_{NaRB} stands for the model of voltage-dependent Na current of Raman and Bean [55]. **B₁**. I_{Nav} replaced by I_{NaRB} with conductance $g_{NaRB} = 5 \times 10^3$ (same as that of I_{Nav} in the standard model). **B₂**. $g_{NaRB} = 3.5 \times 10^3$. **B₃**. $g_{NaRB} = 3 \times 10^3$. **B₄**. Same as **B₃** with $g_{TCN} = 75$ (standard value = 45). **B₅**. With $g_{Kdr} = 1.25 \times 10^4$ (standard value = 4.5×10^3). **B₆**. $g_{NaRB} = 3 \times 10^3$, $g_{Kdr} = 1.25 \times 10^4$ and $g_{TCN} = 9.5 \times 10^1$

introduced in our model. Raman *et al.* [4] fitted their data for the steady-state activation of Na currents with a Boltzmann function of the form given by Eq. (5) for $m_{\text{NaV}\infty}$ (see their Fig. 3C). The standard HH formalism for this current uses the same function but raised to a power of three (see e.g. [26]), i.e. $m_{\text{NaV}\infty}^3$. Assuming that the error between the data points and the model prediction are independently and identically distributed according to a normal law, we computed the Bayesian information criterion (BIC) for both models [56]. We found that $\text{BIC}_{m_\infty} - \text{BIC}_{m_\infty^3} > 16$, which means that the standard $m_{\text{NaV}\infty}^3$ formalism yields a better description of the experimental data than a $m_{\text{Na}\infty}$ formalism. The classical HH formalism hence appears to be capable to describe adequately the transient component of I_{NaV} currents in DCNn. Notice that the two studies on I_{NaV} in DCNn that we are aware of ([4] and [18]) provide divergent results regarding the inactivation parameters of this current. Our model adopts as standard parameters the values reported in [18] in physiological salines rather than values in [4] as the latter were obtained in low external Na conditions. Nevertheless, we found that the basic bifurcation diagram and $F \leftrightarrow \text{SD}$ state transitions are robust to changes in the inactivation parameters of I_{NaV} which include the values reported in [4], thereby showing that these properties do not result from an unrealistically precise setting of the I_{NaV} parameters. We then investigated the possible role of the resurgent component of I_{NaV} reported in DCNn by Afshari *et al.* [18]. This current, which was initially identified in cerebellar Purkinje cells [55], corresponds to a transient block of NaV channels in their open state that is not accounted for by the classical HH formalism. For this reason, we investigated the properties of a variant model in which I_{NaV} was modeled with the state transition scheme of Raman and Bean [19], which produces a resurgent current. Figure 10B summarizes the results of this investigation. When endowed with I_{NaRB} instead of the standard I_{NaV} (same conductance as I_{NaV}), the model can no longer produce $F \leftrightarrow \text{SD}$ transitions due to the loss of overall stability of the FP branch (Fig. 10B₁). The exchange of Na current models also induces the appearance of saddle-node (SN) bifurcation in this branch. Rather than forming an isola of LC as in the standard model, the branch of sLC ends into a homoclinic bifurcation at regular saddle at the left of the bifurcation diagram and into a Hopf bifurcation (H_1) at the right of the diagram. As I_{NaRB} adds a resurgent component to the transient Na current modeled with I_{NaV} , we reasoned that loss of stability of the FP may stem, at least partly, from the Na current having become excessively large. In agreement with this reasoning, panels B₂ and B₃ in Fig. 10 show that a progressive decrease of g_{NaRB} shifts the H_1 point to the left of the bifurcation diagram. It also removes the SN bifurcation point to leave a second Hopf bifurcation point (H_2) which shifts to the right of the bifurcation diagram as g_{NaRB} is decreased furthermore. However, decreasing g_{NaRB} alone proved unable to restore the standard bifurcation diagram as the branch of LCs was lost when the FP resumed overall stability (not illustrated). As our study suggests that the I_{TCN} current contributes to the stability of the FP branch, we then increased g_{TCN} in addition to decreasing g_{NaRB} . Figure 10B₄ shows this additional parameter change brought the H_1 and H_2 closer to each other and allowed the model to recover two short branches of uLC at ends of the branch of sLC. However, further increases in g_{TCN} proved unable for the variant model to recover the isola of LC as they exchanged the stability of the left uLC branch (not illustrated). Given that I_{Kdr} exerts a counteracting effect to I_{Na} , we finally examined the effects of increasing g_{Kdr} . Figure 10B₅ shows that increasing g_{Kdr} has similar effects to that of increasing g_{TCN} . However, increasing g_{Kdr} alone also proved unable for the model to recover the isola of LC (not illustrated). Nevertheless, panel B₆ shows that com-

binning the three effects of decreasing g_{NaRB} and increasing g_{TCN} and g_{Kdr} allows the variant model to recover the overall structure of the bifurcation diagram of the standard model. These results show that a variant model endowed with an accurate biophysical model of I_{NaV} including a resurgent component can produce a bifurcation diagram consistent with that of the standard model and therefore support the mechanism that our study proposes to explain $F \leftrightarrow SD$ transitions of DCNn.

Given that not all DCNn currents have been thoroughly characterized, matching DCNn salient electrophysiological properties (spontaneous spiking frequency, $f-I$ relationship, spikes under- and overshoot values and voltage of the SD state) resulted in trade-off values for parameters of I_{NaV} (i.e. $V_{m\text{NaV}}$, $k_{m\text{NaV}}$, $V_{h\text{NaV}}$, and $k_{h\text{NaV}}$) in our model that deviate from mean experimental values documented in Raman *et al.* [4] and Afhsari *et al.* [18]. Nevertheless, we observed that dynamical properties of our model, including its $F \leftrightarrow SD$ states transitions, could be retained when using these mean experimental values provided that membrane conductances g_{NaV} and g_{TCN} were adjusted in ways that strictly agree with our findings on the effects of these conductances on the bifurcation diagram of the model.

At least two different kinds of DCNn have been characterized: GABAergic DCNn and non-GABAergic DCNn [24]. The former exhibit a lower spontaneous firing frequency (~ 10 vs ~ 30 Hz) and a lower maximal firing frequency than the latter (~ 50 vs > 100 Hz). With standard parameter values, our model has a spontaneous firing frequency of ~ 29 Hz and a maximal frequency of ~ 110 Hz, so our model unambiguously corresponds to non-GABAergic large neurons. From a preliminary exploration of the parameter space, we think that it may be possible to reproduce the firing range of GABAergic DCNn with our model. The spontaneous firing rate mostly depends on the TCN current, so decreasing this conductance leads to a decreased spontaneous firing rate. However, this also alters the bifurcation diagram, destroying the isola of limit cycles and suppressing the possibility of transitions between a firing and a SD state. However, it is not clear if those transitions do arise in GABAergic DCN experimentally. Therefore, our model with its standard parameter values corresponds to non-GABAergic DCNn and further work is needed to determine if it can be adapted to account for GABAergic DCN too.

4.3 Functional implications

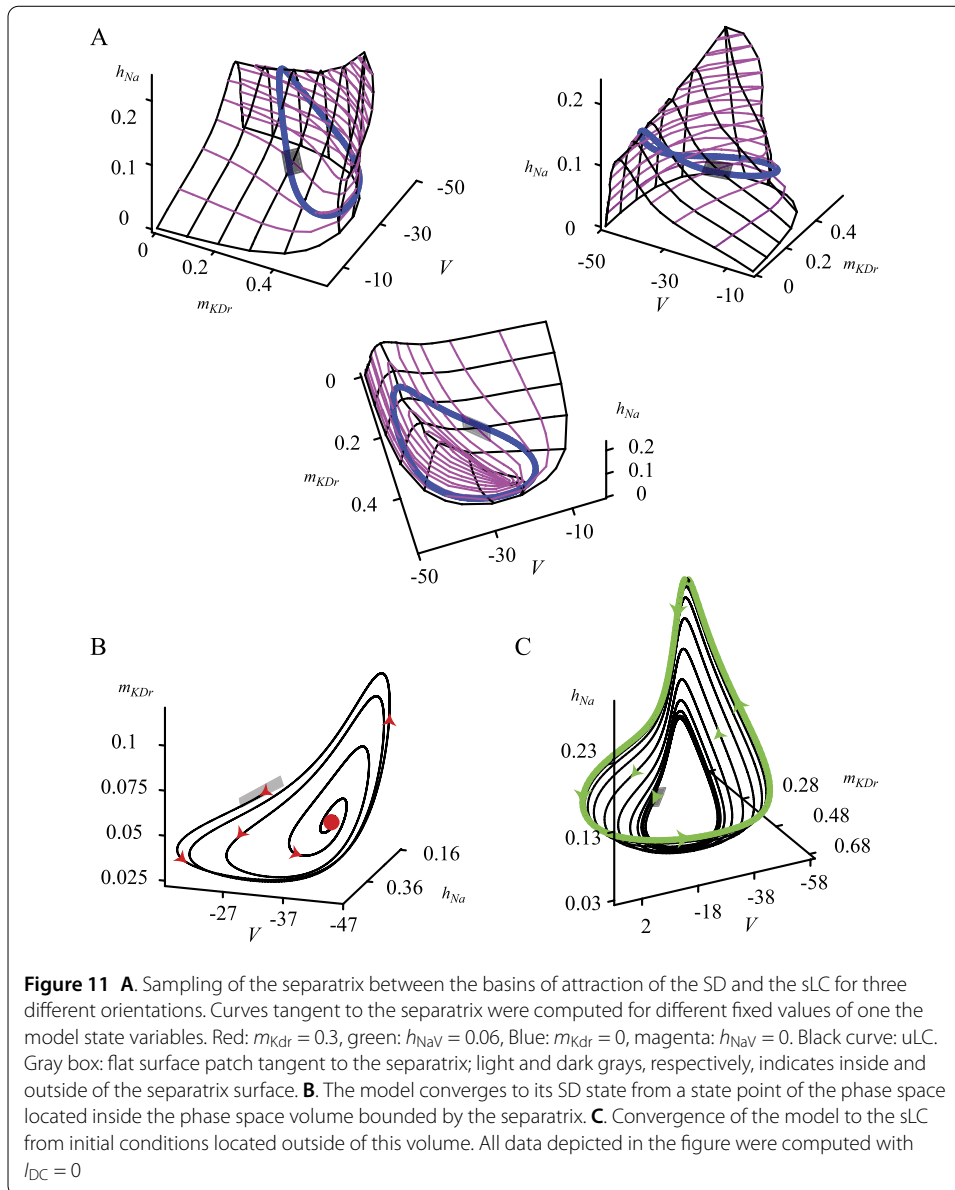
An unresolved central issue in the cerebellum functioning is the observation that activities of connected Purkinje cells (PC) and DCNn can exhibit negative as well as positive correlations [57]. The observation of a positive correlation is puzzling since PC inhibit DCNn (with a ratio of 800 PCs to 1 DCNn) so that one would expect negative correlations between PC and DCNn firings. The basic bifurcation scenario of our DCNn model offers a fresh look at this question. It suggests that salient sensorimotor information transmitted by the phasic inhibitory inputs of Purkinje cells or the excitatory inputs of mossy fibers collaterals can trigger reversible 'on'-'off' transitions of the DCNn (see Fig. 6). According to our model a DCNn can be in its firing 'on' state even if PC targeting it are active provided that the total tonic inhibitory current fed by PC is not large enough to shift the model below the left bound of the isola of limit cycles (see Fig. 2A). Moreover, our model predicts that the state of an initially silent DCNn after a PC inhibitory signal depends on the amplitude of the input: moderate-amplitude inputs will switch the DCNn to its firing state whereas large-amplitude inputs will keep the DCNn in the silent state. Because of this counter-intuitive behavior, the activity of the DCNn and of the PC can exhibit positive and negative correlations, as reported by McDevitt *et al.* [57]. Our findings therefore

strongly suggest to study computational models of the cerebellum network endowed with the basic DCNn state transition features disclosed by our study.

Appendix: On the separatrix between the basins of attraction of the SD and F states

We show in the Methods section that solutions of our model are bounded. Moreover, our model has no strange (fractal dimension) attractor in addition to the F and SD attractors. It follows that any trajectory of the model, whatever its initial conditions, must eventually converge on either the F or the SD attractor. This implies the existence of a closed manifold (i.e. compact and without bounds) separating the phase space. This leads us to propose that the separatrix delimiting the basins of attraction of the F and SD attractors is a $(n - 1)$ -dimension closed manifold. We give here information supporting this hypothesis.

A virtue of the reduced $\{V, m_{Kdr}, h_{NaV}\}$ model is that it possesses a three-dimensional phase space allowing one to visualize its dynamics, contrary to the standard six-dimensional system. We used this property to study in more detail the separatrix between the basins of attraction of the SD and F states. We were able to sample the separatrix in the $\{V, m_{Kdr}, h_{NaV}\}$ model by imposing a fixed value to two its three state variables model and then finding by dichotomy values of the remaining variable that are closest to the separatrix. We illustrate the results in Fig. 11A for three different orientations in the $\{V, m_{Kdr}, h_{NaV}\}$ phase space. The black mesh locates the points of the separatrix sampled for different fixed values of either m_{Kdr} or h_{NaV} . This mesh clearly forms a closed surface showing that the separatrix in the $\{V, m_{Kdr}, h_{NaV}\}$ reduced model is two-dimensional. The small parallelogram in panels A represents a flat surface locally tangent to the separatrix at a point in the phase space with coordinates $(V = -30.1, m_{Kdr} = 0.3, h_{NaV} = 0.06)$. The inner side of this surface is depicted in light gray and its outer side in dark gray. Figure 11B illustrates an example of the fate of all trajectories starting from initial conditions located inside the volume delimited by the separatrix: all these trajectories eventually converge to the SD state (red dot). On the opposite, all trajectories of the model starting from a point located outside of this volume converge onto the sLC (green curve) as illustrated by Fig. 11C. These results confirm that the surface delineated by the black mesh in Fig. 11A₁₋₃ is the separatrix between the attraction basins of the F and SD states. Numerical investigation of the uLC in the $\{V, m_{Kdr}, h_{NaV}\}$ reduced model revealed that this limit cycle has one of its Floquet exponents equal to 1 (as expected from Floquet theory, (see e.g. [13])), a second one being <1 and the remaining one being >1 . Hence, the local unstable manifold of the uLC is of dimension 1 whereas its local stable manifold is of dimension 2. Since the global stable and unstable manifolds of the uLC are locally tangent, respectively, to the local stable and unstable manifolds in a neighborhood of the uLC and according to the above results showing that the separatrix is a closed surface, we are led to propose that the SD/F separatrix is actually the global stable manifold of the uLC. The finding that this manifold is of dimension 2 agrees with the hypothesis that the separatrix is of dimension $n - 1$ in the $\{V, m_{Kdr}, h_{NaV}\}$ reduced model. Moreover, numerical analysis of the uLC in the standard six-dimensional model revealed that one of its Floquet exponents is equal to 1, four of them are <1 and the last one >1 so that the sLC stable manifold is of dimension 5. According to the conclusion derived from the $\{V, m_{Kdr}, h_{NaV}\}$ reduced model, it follows that the F/SD separatrix is likely of dimension 5 in the standard model, thereby providing support for the $n - 1$ dimension hypothesis on the separatrix.



Acknowledgements

We thank Dr. Emmanuel Guigon for fruitful discussions.

Funding

None.

Abbreviations

DCNn, neurons of the deep cerebellar nuclei; F state, firing of spikes state; SD state, stable depolarized state; PC, Purkinje cells; sFP, stable fixed point; sLC, stable limit cycle; uLC, unstable limit cycle; ODE, ordinary differential equations.

Availability of data and materials

Source codes for numerical simulations available upon request to the authors.

Ethics approval and consent to participate

Not applicable.

Competing interests

The authors declare that they have no competing interests.

Consent for publication

Not applicable.

Authors' contributions

SG designed the study; SG and HB analyzed the model and wrote the article. All authors read and approved the final manuscript.

Author details

¹INRIA, 69603 Villeurbanne, France. ²LIRIS UMR5205, Université de Lyon, 69622 Villeurbanne, France. ³Sorbonne Université, CNRS, Institut des Systèmes Intelligents et de Robotique, ISIR, F-75005 Paris, France.

Publisher's Note

Springer Nature remains neutral with regard to jurisdictional claims in published maps and institutional affiliations.

Received: 21 May 2019 Accepted: 17 March 2021 Published online: 01 April 2021

References

1. Llinás R, Muhlethaler M. Electrophysiology of guinea-pig cerebellar nuclear cells in the in vitro brain stem-cerebellar preparation. *J Physiol (Lond)*. 1988;404:241–58.
2. Jahnsen H. Electrophysiological characteristics of neurons in the guinea-pig deep cerebellar nuclei in vitro. *J Physiol (Lond)*. 1986;372:129–47.
3. Aizenman CD, Linden DJ. Regulation of the rebound depolarization and spontaneous firing patterns of deep nuclear neurons in slices of rat cerebellum. *J Neurophysiol*. 1999;82:1697–709.
4. Raman IM, Gustafson AE, Padgett D. Ionic currents and spontaneous firing in neurons isolated from the cerebellar nuclei. *J Neurosci*. 2000;20:9004–16.
5. Zheng N, Raman IM. Ca currents activated by spontaneous firing and synaptic disinhibition in neurons of the cerebellar nuclei. *J Neurosci*. 2009;29:9826–38.
6. Pedroarena CM. Mechanisms supporting transfer of inhibitory signals into the spike output of spontaneously firing cerebellar nuclear neurons in vitro. *Cerebellum*. 2010;9:67–76.
7. Steuber V, Schulteiss NW, Angus Silver R, De Schutter E, Jaeger D. Determinants of synaptic integration and heterogeneity in rebound firing explored with data-driven models of deep cerebellar nucleus cells. *J Comput Neurosci*. 2011;30:633–58.
8. Cooley J, Dodge F, Cohen H. Digital computer solutions for excitable membrane models. *J Cell Comparat Physiol*. 1965;66:99–108.
9. Grimshaw R. Nonlinear ordinary differential equations. Applied mathematics and engineering science texts. Oxford: Blackwell Sci.; 1990.
10. Hassard BD, Shiau LJ. Isolated periodic solutions of the Hodgkin–Huxley equations. *J Theor Biol*. 1989;136:267–79.
11. Rinzel J, Miller RN. Numerical calculation of stable and unstable periodic solutions to the Hodgkin–Huxley equations. *Math Biosci*. 1980;49:27–59.
12. Guttman R, Lewis S, Rinzel J. Control of repetitive firing in squid axon membrane as a model for a neurone oscillator. *J Physiol (Lond)*. 1980;305:377–95.
13. Perko L. Differential equations and dynamical systems. Berlin: Springer; 1996.
14. Gauck V, Thomann M, Jaeger D, Borst A. Spatial distribution of low- and high-voltage activated calcium currents in neurons of the deep cerebellar nuclei. *J Neurosci*. 2001;21:RC158.
15. Womack MD, Khodakhah K. Somatic and dendritic small-conductance calcium-activated potassium channels regulate the output of cerebellar Purkinje neurons. *J Neurosci*. 2003;23:2600–7.
16. Hodgkin AL, Huxley AF. A quantitative description of membrane current and its application to conduction and excitation in nerve. *J Physiol (Lond)*. 1952;117:500–44.
17. Sudhakar SK, Torben-Nielsen B, De Schutter E. Cerebellar nuclear neurons use time and rate coding to transmit Purkinje neuron pauses. *PLoS Comput Biol*. 2015. <https://doi.org/10.1371/journal.pcbi.1004641>.
18. Afshari FS, Ptak K, Khaliq ZM, Grieco TM, Slater NT, McCrimmon R, Resurgent RM. Na current in four classes of neurons of the cerebellum. *J Neurophysiol*. 2004;92:2831–43.
19. Raman IM, Bean BP. Inactivation and recovery of sodium currents in cerebellar Purkinje neurons: evidence for two mechanisms. *Biophys J*. 2001;80:729–37.
20. McKay BE, McRory JE, Molineux ML, Hamid J, Snutch TP, Zamponi GW, Turner RW. Cav3 T-type calcium channels isoforms differentially distribute to somatic and dendritic compartments in rat central neurons. *Eur J Neurosci*. 2006;24:2581–97.
21. Czubayko U, Sultan F, Thier P, Schwartz C. Two types of neurons in the rat cerebellar nuclei as distinguished by membrane potentials and intracellular fillings. *J Neurophysiol*. 2001;85:2017–29.
22. Chan-Palay V. Cerebellar dentate nucleus. Organisation, cytology and transmitters. Berlin: Springer; 1977.
23. Wassef M, Simons J, Tappaz ML, Sotelo C. Non-Purkinje cell GABAergic innervation of the deep cerebellar nuclei: a quantitative immunocytochemical study in C57BL and in Purkinje cell degeneration mutant mice. *Brain Res*. 1986;399:125–35.
24. Uusisaari M, Obata K, Knöpfel T. Morphological and electrophysiological properties of GABAergic and non-GABAergic cells in the deep cerebellar nuclei. *J Neurophysiol*. 2007;97:901–11.
25. Molineux ML, McRory JE, McKay BE, Hamid J, Mehaffey WH, Rehak R, Specific STP. T-type calcium channel isoforms are associated with distinct burst phenotypes in deep cerebellar nuclear neurons. *Proc Natl Acad Sci USA*. 2006;103:5555–60.
26. Hille B. Ionic channels of excitable membranes. Sunderland: Sinauer; 1992.
27. Genet S, Delord B. A biophysical model of nonlinear dynamics underlying plateau potentials and calcium spikes in Purkinje cell dendrites. *J Neurophysiol*. 2002;88:2430–44.
28. Lamont M. An electrophysiological analysis of deep cerebellar nuclei, with particular focus on Kv3 channels. *Biosci Horizons*. 2009. <https://doi.org/10.1093/biohorizons/hzp010>.

29. Huguenard JR, McCormick DA. Simulation of the currents involved in rhythmic oscillations in thalamic relay neurons. *J Neurophysiol.* 1992;68:1373–83.
30. McRory JE, Santi CE, Hamming KSC, Mezeyova J, Sutton KG, Baillie DL, Stea A, Snutch TP. Molecular and functional characterization of a family of rat brain T-type calcium channels. *J Biol Chem.* 2001;276:3999–4011.
31. Gerstner W, Kistler WM, Naud R, Paninski L. *Neuronal dynamics—from single neurons to networks and models of cognition.* Cambridge: Cambridge University Press; 2014.
32. Rudy B, McBain CJ. Kv3 channels: voltage-gated K⁺ channels designed for high-frequency repetitive firing. *Trends Neurosci.* 2001;24:517–26.
33. Liu PW, Bean BP. Kv2 channel regulation of action potential repolarization and firing patterns in superior cervical ganglion neurons and hippocampal CA1 pyramidal neurons. *J Neurosci.* 2014;34:4991–5002.
34. Coetzee W, Amarillo Y, Chiu J, Chow A, Lau D, McCormack T, Moreno H, Nadal M, Ozaita A, Pountney D, Saganich M, Vega-Saenz de Miera E, Rudy B. Molecular diversity of K⁺ channels. *Ann NY Acad Sci.* 1999;868:233–85.
35. Weiser M, Bueno E, Sekirnjak C, Martone ME, Baker H, Hillman D, Chen S, Thornhill W, Ellisman M, Rudy B. The potassium channel subunit KV3.1b is localized to somatic and axonal membranes of specific populations of CNS neurons. *J Neurosci.* 1995;15:4298–314.
36. Helton TD, Xu W, Lipscombe D. Neuronal L-type calcium channels open quickly and are inhibited slowly. *J Neurosci.* 2005;25:10247–51.
37. Destexhe A, Neubig M, Ulrich D, Huguenard J. Dendritic low-threshold calcium currents in thalamic relay cells. *J Neurosci.* 1998;18:3574–88.
38. Smirnov V. *Cours de mathématiques supérieures. Tome 2.* Moscow: Mir; 1979.
39. Dillon PF. *Biophysics: a physiological approach.* Cambridge: Cambridge University Press; 2012.
40. Cronin J. *Mathematical aspects of Hodgkin–Huxley neural theory.* Cambridge studies in mathematical biology. Cambridge: Cambridge University Press; 1987.
41. Rinzel J, Ermentrout B. Analysis of neural excitability and oscillations in methods. In: Koch C, Segev I, editors. *Neuronal modeling;* 1989.
42. Hodgkin AL. The local electric changes associated with repetitive action in a non-medulated axon. *J Physiol (Lond).* 1948;107:165–81.
43. Izhikevich EM. *Dynamical systems in neuroscience. The geometry of excitability and bursting.* Sejnowski TJ, Poggio TA, editors. Cambridge: MIT Press; 2007.
44. Avitabile D, Desroches M, Rodrigues S. On the numerical continuation of isolas of equilibria. *Int J Bifurc Chaos.* 2012. <https://doi.org/10.1142/S021812741250277X>.
45. Labouriau IS. Degenerate Hopf bifurcation and nerve impulse. *SIAM J Math Anal.* 1985;16:1121–33.
46. Labouriau IS. Degenerate Hopf bifurcation and nerve impulse. Part II. *SIAM J Math Anal.* 1989;20:1–12.
47. Bean BP. Classes of calcium channels in vertebrate cells. *Annu Rev Physiol.* 1989;51:367–84.
48. Fitzhugh R. Thresholds and plateaus in the Hodgkin–Huxley nerve equations. *J Gen Physiol.* 1960;43:867–96.
49. Fitzhugh R. Impulses and physiological states in models of nerve membrane. *Biophys J.* 1961;1:445–66.
50. Rinzel J. Excitation dynamics: insights from simplified membrane models. *Fed Proc.* 1985;44:2944–6.
51. Jahnsen H. Extracellular activation and membrane conductances of neurons in the guinea-pig deep cerebellar nuclei in vitro. *J Physiol (Lond).* 1986;372:149–68.
52. Boehme R, Uebele VN, Renger JJ, Pedroarena C. Rebound excitation triggered by synaptic inhibition in cerebellar nuclear neurons is suppressed by T-type calcium channels block. *J Neurophysiol.* 2011;106:2653–61.
53. Grace AA, Bunney BS. Induction of depolarization block in midbrain dopamine neurons by repeated administration of haloperidol: analysis using in vivo intracellular recording. *J Pharmacol Exp Ther.* 1986;238:1092–100.
54. Bianchi D, Marasco A, Limongiello A, Machetti C, Marie H, Tirozzi B, Migliore M. On the mechanisms underlying the depolarization block in the spiking dynamics of CA1 pyramidal neurons. *J Comput Neurosci.* 2012;33:207–25.
55. Raman IM, Bean BP. Resurgent sodium current and action potential formation in dissociated cerebellar Purkinje neurons. *J Neurosci.* 1997;17:4517–26.
56. Schwarz GE. Estimating the dimension of a model. *Ann Stat.* 1978;6:461–4.
57. McDevitt CJ, Ebner TJ, Bloedel JR. Relationships between simultaneously recorded Purkinje cells and nuclear neurons. *Brain Res.* 1987;425:1–13.

Submit your manuscript to a SpringerOpen[®] journal and benefit from:

- Convenient online submission
- Rigorous peer review
- Open access: articles freely available online
- High visibility within the field
- Retaining the copyright to your article

Submit your next manuscript at ► [springeropen.com](https://www.springeropen.com)
